

REVIEW OF LOW-TEMPERATURE OXIDATION OF CARBON STEELS AND LOW-ALLOY STEELS FOR USE AS HIGH-LEVEL RADIOACTIVE WASTE PACKAGE MATERIALS

Prepared for

**Nuclear Regulatory Commission
Contract NRC-02-93-005**

Prepared by

**Center for Nuclear Waste Regulatory Analyses
San Antonio, Texas**

February 1997



**REVIEW OF LOW-TEMPERATURE OXIDATION OF CARBON
STEELS AND LOW-ALLOY STEELS FOR USE AS HIGH-LEVEL
RADIOACTIVE WASTE PACKAGE MATERIALS**

Prepared for

**Nuclear Regulatory Commission
Contract NRC-02-93-005**

Prepared by

**Sylvain Larose and Robert A. Rapp
The Ohio State University
Columbus, Ohio**

for the Center for Nuclear Waste Regulatory Analyses

February 1997

PREVIOUS REPORTS IN SERIES

Number	Name	Date Issued
CNWRA 91-004	A Review of Localized Corrosion of High-Level Nuclear Waste Container Materials—I	April 1991
CNWRA 91-008	Hydrogen Embrittlement of Candidate Container Materials	June 1991
CNWRA 92-021	A Review of Stress Corrosion Cracking of High-Level Nuclear Waste Container Materials—I	August 1992
CNWRA 93-003	Long-Term Stability of High-Level Nuclear Waste Container Materials: I—Thermal Stability of Alloy 825	February 1993
CNWRA 93-004	Experimental Investigations of Localized Corrosion of High-Level Nuclear Waste Container Materials	February 1993
CNWRA 93-014	A Review of the Potential for Microbially Influenced Corrosion of High-Level Nuclear Waste Containers	June 1993
CNWRA 94-010	Review of Degradation Modes of Alternate Container Designs and Materials	April 1994
CNWRA 94-028	Environmental Effects on Stress Corrosion Cracking of Type 316L Stainless Steel and Alloy 825 as High-Level Nuclear Waste Container Materials	October 1994
CNWRA 95-010	Experimental Investigations of Failure Processes of High-Level Radioactive Waste Container Materials	May 1995
CNWRA 96-004	Thermal Stability and Mechanical Properties of High-Level Radioactive Waste Container Materials: Assessment of Carbon and Low-Alloy Steels	May 1996

ABSTRACT

For the proposed high-level waste (HLW) repository site at Yucca Mountain, Nevada, the outer surface of the buried waste containers is expected to be exposed to dry atmospheres for thousands of years at temperatures slowly decreasing from 300 °C. In this report, the expected oxidation behavior of the candidate materials for the outer overpack of the containers, carbon steels and Fe-2.25Cr-1Mo steels, was estimated for a period of 1,000 years for temperatures in the range 100–300 °C. In dry atmospheres in this low-temperature range, the candidate steels form scales consisting of only two oxide phases: α -Fe₃O₄ and Fe₂O₃. After a relatively short transient period, the oxidation kinetics follow a parabolic rate law, which has been used for extrapolation to very long times. However, most previous studies have been done at higher temperatures and certainly for shorter times than the proposed waste container application.

The extrapolation of the existing data according to a parabolic kinetics law with an Arrhenius temperature dependence assumes that the scale growth kinetics are limited by solid-state (grain boundary) diffusion through a dense uniform scale. The scaling rates of low-carbon steels at 200–350 °C increase with increases in carbon content and fineness of the Fe₃C dispersion in ferrite. Upon extrapolation of the oxidation kinetics to 1,000 years at 250 °C, an abraded 0.2 wt% C steel having a fine pearlitic microstructure is expected to suffer only 4.1 μ m of oxidation. Even less metal recession is expected for carbon steels with spheroidized C and a chemically etched surface. Neither decarburization of carbon steels upon oxidation nor any significant preferential grain boundary attack of the HLW canisters is expected to occur at such low temperatures.

In the case of Fe-2.25Cr-1Mo steels, the oxidation studies found in the literature were conducted only at 500 °C and higher. So the extrapolation of the data to much lower temperatures and for very long times is somewhat precarious. For 1,000 years of dry oxidation at 250 °C, abraded Fe-2.25Cr-1Mo steels are expected to recede only 2.1 μ m. Cold work of the surfaces by abrasion leads to a better contact between the steel and the oxide scale, but also to a higher oxidation rate. In fact, for such very thin oxide films, cracking and spallation are not expected to occur. Where data were available, predictions of times for scale rupture resulting in breakaway oxidation were also made, but this phenomenon is not significant at such low temperatures. The literature provides insight about the dependences of the oxidation behavior on the composition, tempering treatment, microstructure, and the surface preparation of the steels.

The data analyzed in this report indicate that carbon steels and low alloy steels have very similar very slow oxidation kinetics at low temperature for extended periods of time. Therefore, either Fe-0.2 wt% C steel with spheroidized carbide, or low-C, large grain (60 μ m or more) Fe-2.25Cr-1Mo steel with optimum heat treatment are good choices of materials for the outer containment barrier of the HLW containers. Chemical etching/polishing would serve to minimize the oxidation kinetics. A further preliminary surface treatment, optimized to instigate the "Reactive Element Effect," to further minimize the scaling rate and improve scale adherence is also discussed.

CONTENTS

Section	Page
FIGURES	vii
TABLES	ix
ACKNOWLEDGMENTS	xi
1 INTRODUCTION	1-1
2 OXIDATION OF PURE IRON IN DRY AIR AND OXYGEN	2-1
3 CARBON STEELS	3-1
4 OXIDATION OF Fe-2.25Cr-1Mo IN DRY AIR AND OXYGEN	4-1
5 POSSIBILITY TO REDUCE THE SCALING RATE	5-1
5.1 REACTIVE ELEMENT EFFECT	5-1
5.2 MECHANISMS FOR THE REACTIVE ELEMENT EFFECT	5-1
5.3 APPLICATION OF REACTIVE ELEMENT EFFECT TO STEEL CONTAINERS	5-4
6 SUMMARY, CONCLUSIONS, AND RECOMMENDATIONS	6-1
7 REFERENCES	7-1

FIGURES

Figure		Page
2-1	Phase relations and stabilities for partial iron-oxygen system; first representation (Muan and Osborn, 1965)	2-2
2-2	Oxygen partial pressure as a function of P_{CO}/P_{CO_2} ratio	2-3
2-3	Oxygen partial pressure as a function of the P_{H_2}/P_{H_2O} ratio	2-3
2-4	Phase relations and stabilities for partial iron-oxygen system; second representation (Pourbaix et al., 1996)	2-4
2-5	Schematic illustration of the cation flux partitioning at the Fe_3O_4/Fe_2O_3 interface during the low temperature oxidation of iron	2-5
2-6	Influence of cold work on the oxidation rate of pure iron (Caplan and Cohen, 1966).	2-5
3-1	Effect of carbon concentration on the oxidation of iron-carbon alloys at 500 °C at a P_{O_2} of 0.01 atm (Boggs and Kachik, 1969)	3-3
3-2	Effect of carbon concentration on the oxidation of iron-carbon alloys at 500 °C at a P_{O_2} of 0.92 atm (Boggs and Kachik, 1969)	3-3
3-3	Parabolic plots for the oxidation of a Fe-1 wt% C alloy at 500 °C (Boggs and Kachik, 1969)	3-4
3-4	Oxidation curves for three Fe-C alloys at 500 °C (Caplan et al., 1978)	3-6
3-5	Instantaneous parabolic growth rate constants, k_p , plotted against time for Fe-C alloys oxidized at 500 °C in $P_{O_2} = 1$ atm (Caplan et al., 1978)	3-6
3-6	Semi-logarithmic plots of oxidation of pearlitic carbon steels containing various amounts of carbon at a temperature of 350 °C and oxygen partial pressure of 0.13 atm (Runk and Kim, 1970)	3-8
3-7	Parabolic plots of oxidation of pearlitic carbon steels containing various amounts of carbon at a temperature of 350 °C and oxygen partial pressure of 0.13 atm (replotted from the data of Runk and Kim, 1970)	3-9
3-8	Logarithmic plots of oxidation of pearlitic carbon steels containing 0.8 wt% carbon and having three distinct microstructures (fine pearlite, coarse pearlite, and spheroidite) at 350 °C under an oxygen partial pressure of 0.13 atm (Runk and Kim, 1970)	3-11
3-9	Parabolic plots of oxidation of pearlitic carbon steels containing 0.8 wt% carbon and having three distinct microstructures (fine pearlite, coarse pearlite, and spheroidite) at 350 °C under an oxygen partial pressure of 0.13 atm (Runk and Kim, 1970)	3-12
3-10	Logarithmic plots showing the influence of temperature on the oxidation rate of a pearlitic carbon steel containing 0.8 wt% carbon at an oxygen partial pressure of 0.13 atm (Runk and Kim, 1970)	3-14
3-11	Parabolic plot of oxidation of a pearlitic carbon steel containing 0.8 wt% carbon oxidized at 250 °C under an oxygen partial pressure of 0.13 atm (Runk and Kim, 1970)	3-15
3-12	Parabolic plot of oxidation of pearlitic carbon steels containing 0.8 wt% carbon oxidized at 300 and 350 °C under an oxygen partial pressure of 0.13 atm (Runk and Kim, 1970)	3-16

FIGURES (cont'd)

Figure		Page
3-13	Influence of phase boundary length on the oxidation rate at 300 °C for two-phase, Fe-Fe ₃ C substrate of Fe-0.8 wt% C with fine pearlite morphology (Runk and Kim, 1970)	3-17
4-1	Nelson diagram for operating limits of steels in pressurized hydrogen in one-year service (Prescott, 1980)	4-2
4-2	Micrograph showing the various layers of oxidized Fe-2.25Cr-1Mo (Simms and Little, 1987)	4-4
4-3	Temperature-dependence of the parabolic rate constants during the oxidation of Fe-2.25Cr-1Mo in dry oxygen (Simms and Little, 1987)	4-6
4-4	Oxidation of Fe-2.25Cr-1Mo in dry-flowing oxygen for periods up to 100 hours. (A) 550 °C. (B) 600 °C. (C) 650 °C. (D) 700 °C (from Simms and Little, 1987) . . .	4-8
4-5	Variation in composition of M ₆ C on tempering at 700 °C; (a) steel with 0.18% C, (b) steel with 0.06% C (Pilling and Ridley, 1982)	4-10
4-6	Variation in composition of M ₂ C on tempering at 700 °C; (a) steel with 0.18% C, (b) steel with 0.06% C, (c) steel with 0.09% C (Pilling and Ridley, 1982)	4-11
4-7	Acoustic emission (AE) signals of samples that were oxidized in air at temperatures in the range from 600–950 °C and cooled down to room temperature (Khanna et al., 1985)	4-12
5-1	Oxidation kinetics of unimplanted and implanted (with 10 ¹⁶ ion/cm ² Ce) Ni-30 Cr alloys at 1,000 °C in a 80 mole percent (m/o) CO:20 m/o CO ₂ Gas Mixture (Patibandla et al., 1991)	5-2
5-2	Weight gain per unit area as a function of time showing the influence of the dose of implanted Yttrium on the rate of oxidation of a Co-45Cr alloy at 1,000 °C in pure oxygen (Przybylski et al., 1988)	5-3
5-3	Oxidation kinetics at 1100 °C of a Fe-25Cr base alloy and a base alloy coated with 2, 4, 20, and 30 nm CeO ₂ (Hussey et al., 1989)	5-3
5-4	Schematic representation of the “poisoned-interface” interpretation of the reactive element effect (Strawbridge and Rapp, 1994)	5-5
5-5	Trends in reduction of weight gain (compared with uncoated samples) after oxidation in 1 atm O ₂ for 24 h for pure metals with evaporated coatings of 250 Å Ba, Ca, or Sr. Oxidation at 1,000 °C for Ni, 750 °C for Fe, and 500 °C for Cu. (Strawbridge and Rapp, 1994)	5-6
5-6	Oxidation kinetics for pure Ni coupons with and without 250 Å films of Ca, in 1 atm O ₂ at 850 °C: (a) Weight gain with time; (b) Pieraggi plot (Strawbridge and Rapp, 1994)	5-6

TABLES

Tables	Page
3-1	Chemical composition of A516 Grade 55 steel 3-1
3-2	Oxidation rate constants at 350 °C and at a P _{O₂} of 0.13 atm for Fe-C alloys with fine pearlite and various carbon contents (Runk and Kim, 1970) 3-7
3-3	Mass gain per unit area ($\Delta m/A$), thickness of the oxide scale (X), and recession thickness (R) calculated for a period of 1,000 years of oxidation of Fe-C alloys with fine pearlite at 350 °C and at a P _{O₂} of 0.13 atm 3-10
3-4	Oxidation rate constants at 350 °C at a P _{O₂} of 0.13 atm for Fe-0.8 wt% C alloys with various microstructures (Runk and Kim, 1970). Values in parentheses correspond to Fe-0.2 wt% C alloy. 3-13
3-5	Mass gain per unit area ($\Delta m/A$), thickness of the oxide scale (X), and recession depth (R) calculated for a period of 1,000 years of oxidation of Fe-0.8 wt% C at 350 °C at a P _{O₂} of 0.13 atm. Values in parentheses correspond to Fe-0.2 wt% C alloy. 3-13
3-6	Mass gain per unit area ($\Delta m/A$), thickness of the oxide scale (X), and recession thickness (R) calculated for Fe-0.8 wt% C with fine pearlite for a period of 1,000 years in 0.13 atm of dry oxygen. Values in parentheses correspond to Fe-0.2 wt% C alloy. 3-13
4-1	Chemical composition of A387 Grade 22 steel 4-1
4-2	Parabolic rate constants and estimated breakaway times calculated with the data of Simms and Little (1987) obtained in dry oxygen in the temperature range 550–700 °C. 4-5
4-3	Mass gain per unit area ($\Delta m/A$), thickness of the oxide scale (X), and recession thickness (R) calculated for a period of 1,000 years of oxidation in dry oxygen 4-7

ACKNOWLEDGMENTS

This report was prepared to document work performed by the Center for Nuclear Waste Regulatory Analyses (CNWRA) for the Nuclear Regulatory Commission (NRC) under Contract No. NRC-02-93-005. The activities reported here were performed on behalf of the NRC Office of Nuclear Material Safety and Safeguards (NMSS), Division of Waste Management (DWM). The report is an independent product of the CNWRA and does not necessarily reflect the views or regulatory position of the NRC. Sources of data are referenced in each chapter. The respective sources should be consulted for determining their levels of quality assurance.

The authors acknowledge the comments of Gustavo Cragolino to the draft of this report, the technical review of Hersh Manaktala, and the programmatic review of Budhi Sagar. Appreciation is due to Bonnie L. Garcia for her assistance in the preparation of this report.

1 INTRODUCTION

The choice of a material to make containers for high-level nuclear wastes (HLW) is an extremely important matter because of the very long period of time (1,000 years or more) during which these components must provide containment for the HLW from the environment. Alloys are the materials of choice for this application because of their fabricability, ductility, toughness, and the ease by which large containers can be made. Alloy components can usually be welded to provide gas-tight seals that are resistant to degradation. Various metals and their alloys have been investigated for use in nuclear waste containers, such as iron and steels, nickel and nickel-base alloys, copper and copper-base alloys, and titanium (Nuttall and Urbanic, 1981; Van Konynenburg et al., 1993). Iron-base materials such as low-alloy steels, and especially carbon steels, are candidate materials because of their low cost which allows the use of thicker sections than for other alloys. The thick sections provide added strength, they decrease the intensity of any radiolytic effects on the environment, and they increase the service life in the environment without perforation of the container by oxidation.

In the proposed Yucca Mountain, Nevada, repository project, the current design of the HLW containers consists of a thick (10 cm) outer overpack made of carbon steel or low-alloy steel, surrounding a thinner (2 cm) inner overpack made of a Ni-base alloy, which itself surrounds an inner multipurpose canister made of type 316L stainless steel (3.5 cm thick) containing the spent fuel assemblies (TRW Environmental Safety Systems, Inc., 1996). The repository at Yucca Mountain will be located well above the water table. Also, the surrounding geology and local climate are such that the ambient relative humidity is low and significant liquid water is not expected to come into contact with the HLW containers during the heating period of the repository which may extend to hundreds of years. The temperature at the surface of the outer container is expected to decrease slowly from 300 °C to 150 °C over a period of 1,000 years (TRW Environmental Safety Systems, Inc., 1995) because of the decrease in the heat flux generated by the nuclear activity of the HLW. These warm temperatures will further reduce the relative humidity at the surface of the outer container. As a result, the primary degradation mechanism of this container during the initial hot and dry period is expected to be "low-temperature, dry oxidation."

Three main factors affecting the corrosion or oxidation of the outer surface of a metallic container are the nature of the surrounding environment, the design of the container, and the composition and microstructure of the alloy. For a given environment and design, the variable that determines the rate of dry oxidation is the composition of the outer container material. The purpose of this report is to critically review the literature pertaining to the low temperature oxidation of iron, carbon steels and low-alloy steels as candidate materials for the outer overpack.

2 OXIDATION OF PURE IRON IN DRY AIR AND OXYGEN

The oxidation of pure iron is considered before describing alloy oxidation. Iron of high purity shows a high resistance to oxidation. At room temperature in rural atmospheres, pure iron shows a higher resistance to rusting than mild (low-carbon) steels (Craig, 1989). When the relative humidity falls below 60 percent, the rusting of iron becomes extremely slow and a stable oxide film reaches a maximum thickness of a few nm (Davis, 1996). But the oxidation of pure iron becomes more significant in industrial or saline atmospheres and at higher temperatures. The problem of the high temperature oxidation of iron can be approached by first considering the FeO-Fe₂O₃ phase diagram (Muan and Osborn, 1965). This diagram, given in Figure 2-1, illustrates the phase relations and thermodynamic oxygen activities as a function of temperature. The dashed lines in Figure 2-1 plot the equilibrium oxygen activities as a function of composition and temperature. While these activities seem to indicate unrealistically low partial pressures, the thermodynamically equivalent CO/CO₂ or H₂/H₂O ratios are readily realized, as seen in Figures 2-2 and 2-3 (Rapp, 1980). These diagrams show that three iron oxides exist in the Fe-O system: the metal-deficient monoxide wustite (Fe_{1-y}O), the inverse spinel magnetite (Fe₃O₄), and hematite (α -Fe₂O₃) with the corundum structure. While magnetite and hematite are thermodynamically stable from room temperature to ~1600 °C, wustite is stable only from 567 °C to ~1400 °C. Another representation of the phase equilibria between iron and oxygen is given in Figure 2-4 (Pourbaix et al., 1996) where the ranges of stability of the phases are plotted as function of the oxygen partial pressure and temperature. Knowledge of the iron-oxygen equilibrium is important for the interpretation of the oxidation mechanism of iron. If a metal such as iron can form several oxides, for local equilibrium across the oxide scale, the most oxygen-deficient oxide must exist adjacent to the metal and the most oxygen-rich phase must be in contact with the gas phase. For oxidation in air below 567 °C, the scale consists of only two layers with the more iron-rich oxide, magnetite, next to the metal, and the more oxygen-rich oxide, hematite, in contact with the gas phase. Oxygen potential lines, such as those drawn in Figures 2-1 and 2-4, provide values for the oxygen activity at the interfaces of coexisting phases at a given temperature. For a scale sequence in a binary system, such as Fe-O, flat interfaces are stable, and the oxygen activity gradient through the scale is continuous. With the introduction of alloying elements, even without the formation of a new oxide phase, the phase interfaces can become irregular as the additional component provides an alloying thermodynamic degree of freedom.

The relative thicknesses of several scale phases in sequence have been treated by many authors (Wagner, 1969; Yurek et al., 1974; Viani and Gesmundo, 1980; Fromhold and Sato, 1981; Fromhold, 1982; Hsu, 1986; Wang et al., 1989). In general, the advance (growth) of an inner scale layer by cation diffusion is decided by the partitioning of the cation flux through the inner layer to diffusion in the next scale layer and to growth of the trailing phase. Thus, the relative thicknesses of magnetite and hematite formed at temperatures below 567 °C depend upon the relative iron diffusion rates and the compositions of the Fe oxides, as shown schematically in Figure 2-5. Grain boundaries are known to affect significantly the ionic diffusivities in oxides, especially as the temperature is lowered. Because the iron and oxygen ion self-diffusion coefficients in polycrystalline hematite are not available, the theoretical prediction of the relative thicknesses of hematite and magnetite is not possible. On the other hand, excellent volume diffusion data from Dieckmann and Schmalzried (1977) are available for magnetite for high temperatures. But in the absence of grain boundary diffusion coefficients in magnetite at low temperatures, one must rely on experimentally measured scaling kinetics and observed relative scale thicknesses.

The oxidation of pure iron between 400 and 550 °C is especially influenced by the formation of cracks (microscopic detachment) at the metal/scale interface. These cracks result from vacancy condensation in

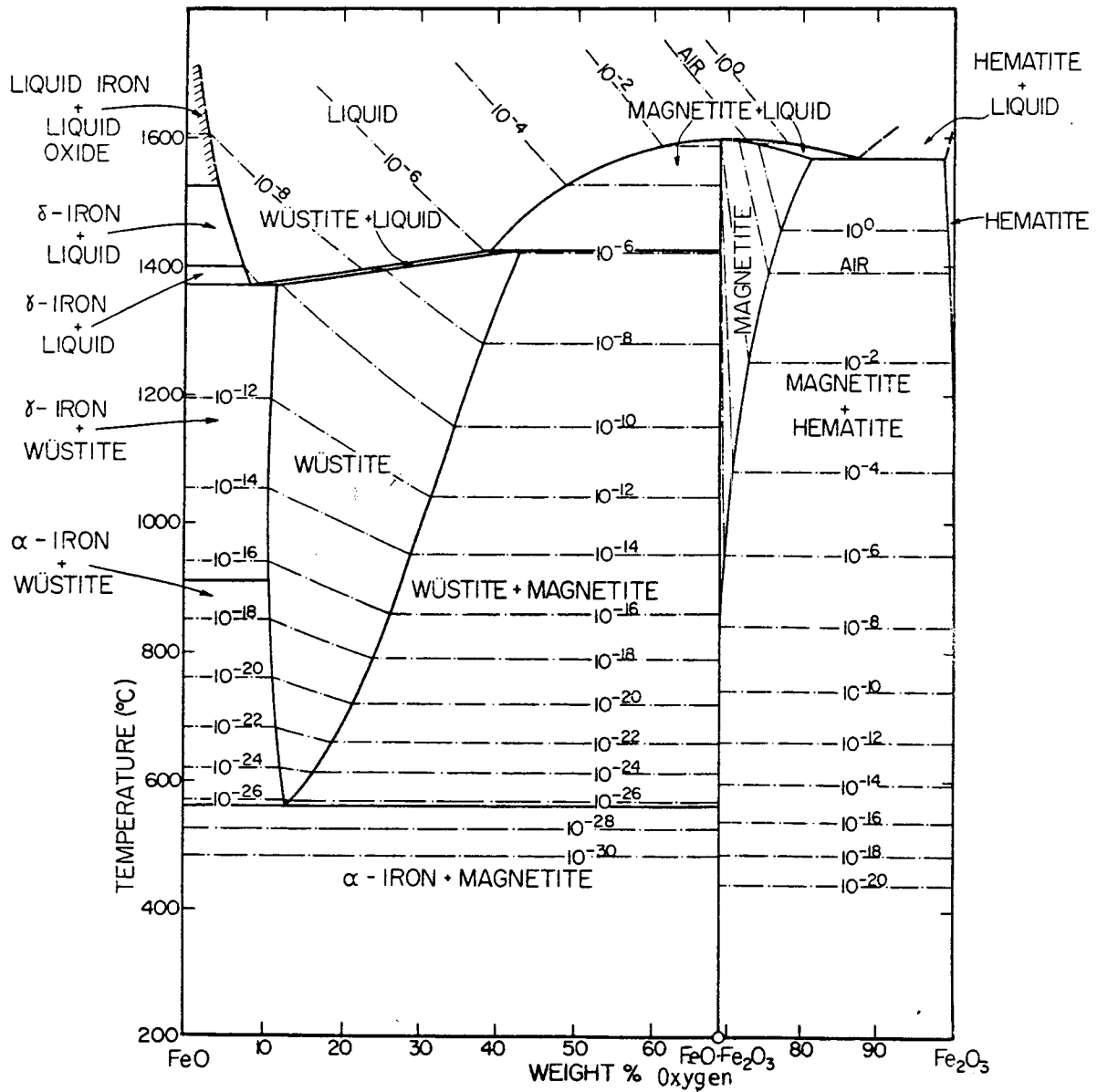


Figure 2-1. Phase relations and stabilities for partial iron-oxygen system; first representation [Muan and Osborn (1965), reprinted with permission from Addison-Wesley Longman, Inc.]

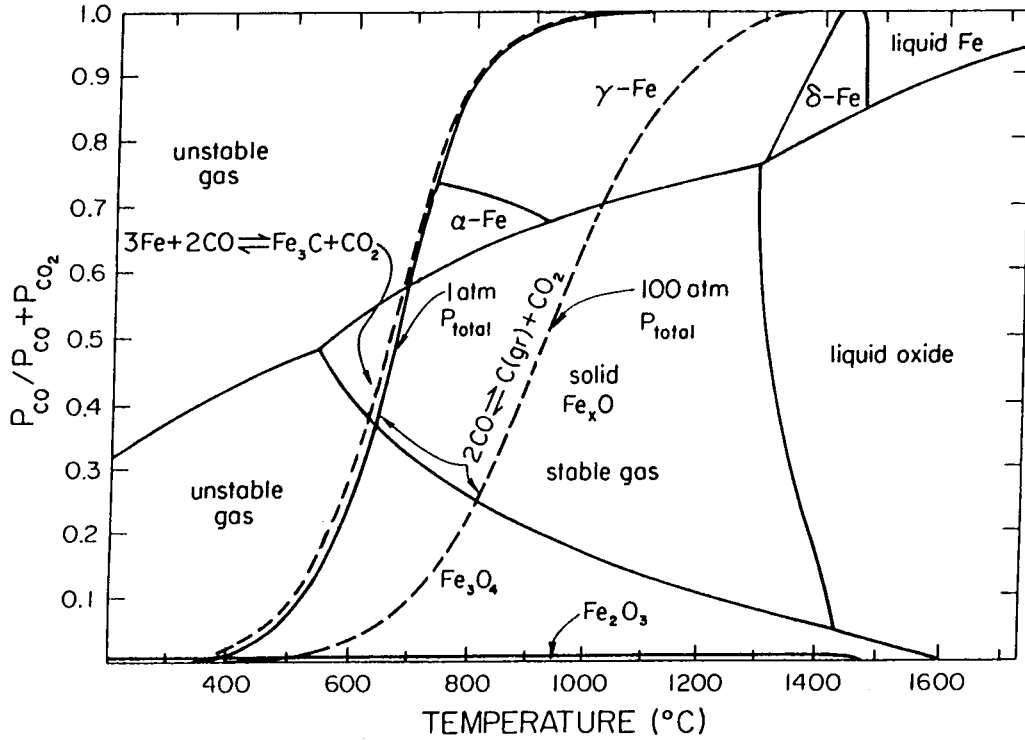


Figure 2-2. Oxygen partial pressure as a function of P_{CO}/P_{CO_2} ratio (Rapp, 1980)

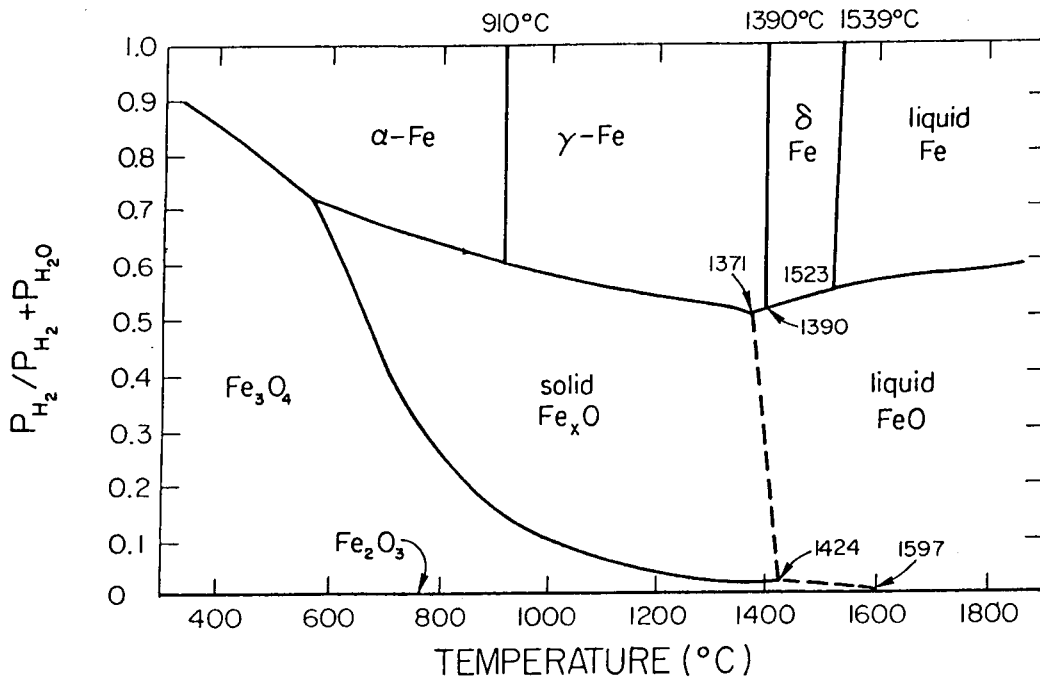


Figure 2-3. Oxygen partial pressure as a function of the P_{H_2}/P_{H_2O} ratio (Rapp, 1980)

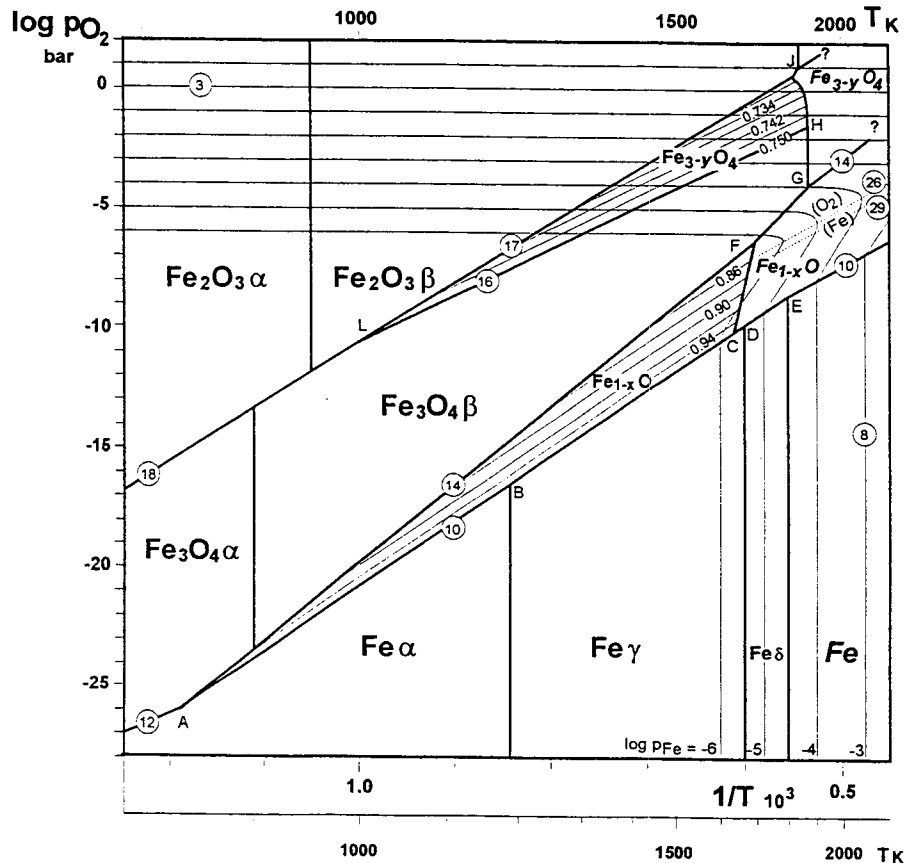


Figure 2-4. Phase relations and stabilities for partial iron-oxygen system; second representation [Pourbaix et al. (1996), reprinted with permission from CEBELCOR, Belgian Center for Corrosion Study]

the interface (Caplan and Cohen, 1963; Caplan et al., 1970a; Hussey and Cohen, 1971a), especially because magnetite exhibits negligible plasticity (Mackenzie and Birchenall, 1957). Such behavior is related to the outward growth of the scale and the receding metal core. Therefore, the loss of scale adherence depends upon the curvature of the surface, with a flat plate or a surface with concave curvature exhibiting a lesser problem than one with convex curvature (e.g., a wire or sphere). The local metal/scale separation leads to unusual kinetic phenomena and to an anomalous effect of oxygen pressure (Caplan et al., 1970a; Hussey and Cohen, 1971b). Because of the disturbed contact of the metal and the scale, the scale thickness and composition are locally irregular.

In the 400–550 °C temperature regime, iron oxidation is influenced strongly by cold working (abrasion) of the metal surface (Caplan and Cohen, 1966; Price, 1967; Caplan et al., 1970b). Surface abrasion prevents or delays the local separation of the scale from the metal. The improved adherence is rationalized as resulting from the higher dislocation density in the metal, such that vacancy annihilation can occur by dislocation climb within the metal rather than forming voids in the interface. The oxidation of cold-worked iron then obeys parabolic, faster, scaling kinetics than undeformed metal. The oxide for the abraded substrate is more uniform in thickness and composition, and the principal scale is Fe₃O₄. The influence of cold work is shown in Figure 2-6 (Caplan and Cohen, 1966). Local detachment of a very

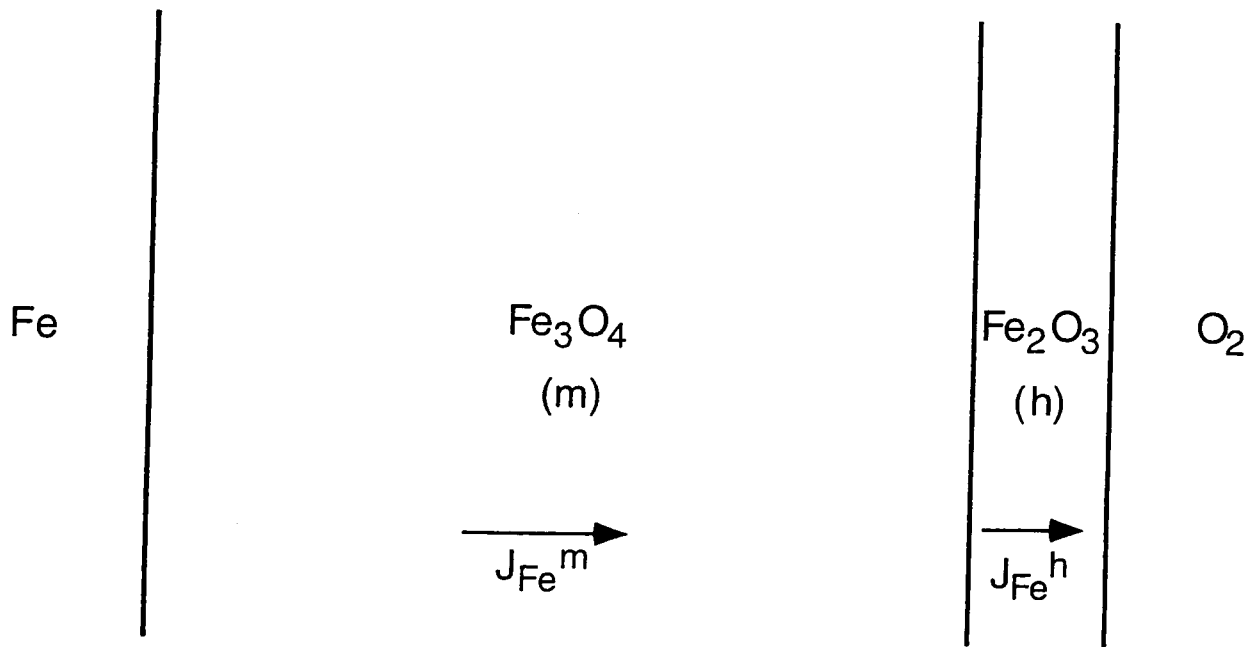


Figure 2-5. Schematic illustration of the cation flux partitioning at the Fe₃O₄/Fe₂O₃ interface during the low temperature oxidation of iron

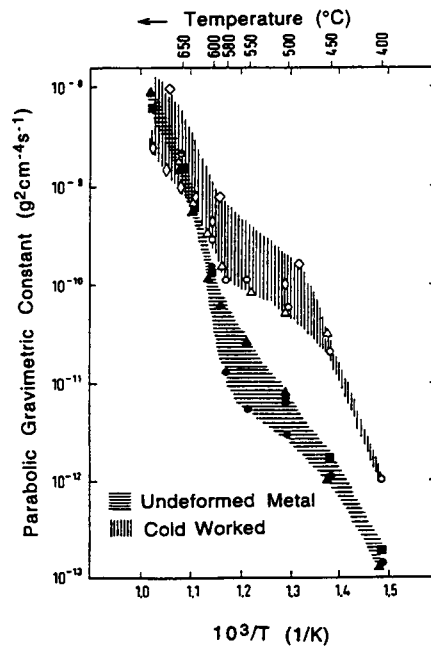


Figure 2-6. Influence of cold work on the oxidation rate of pure iron. The diagram clearly shows that the scaling kinetics of cold worked iron are faster than those of undeformed metal for temperatures below 650 °C. [Caplan and Cohen (1966), reprinted with permission from Elsevier Science Ltd.]

thin oxide scale seldom induces spallation or local cracking. Therefore, such detachment would help reduce the oxidation kinetics by impeding the outward cationic diffusion through the scale.

At lower temperatures (e.g., 350 °C) and lower oxygen pressures, magnetite forms at the start of oxidation, and the nucleation of α -Fe₂O₃ is delayed (Hussey and Cohen, 1971a; Graham and Cohen, 1969; Boggs et al., 1965; Boggs et al., 1967). Since the Fe₃O₄/Fe₂O₃ equilibrium oxygen pressure lies below that of the oxidizing gas, the eventual formation of a continuous external Fe₂O₃ layer reduces the gradient across the magnetite and thereby lowers the oxidation rate. However, this phenomenon occurs in a matter of minutes or a few hours, and would not be important to the container oxidation problem.

At temperatures around 200 °C, the early kinetics and mechanism of iron oxidation are changed (Vernon et al., 1953; Davies et al., 1954; Grauer and Feitknecht, 1966; Simmons et al., 1973). While above 200 °C a parabolic rate law is obeyed, below 200 °C a logarithmic oxidation rate is observed. The oxidation leads to the formation of a product film of about 10⁻⁵ cm thickness. The weight gain data obtained by Davies et al. (1954) in the temperature range 175–350 °C were used by Uhlig (1956) to calculate an activation energy of 29 kJ/mol (0.30 eV) for the logarithmic oxidation of pure iron. The results of Davies et al. (1954) indicate that this rate law applies during the entire duration of the experiments (i.e., 8 hours). Obviously, such a short experiment cannot provide insight to the oxidation behavior for the extremely long service lives for the HLW containers.

3 CARBON STEELS

Use of the term "carbon steel" usually implies that one or more of the following conditions is met (Craig, 1989):

- The steel contains up to 1 wt% C.
- No minimum content is specified or required for aluminum (except as related to deoxidation or grain-size control), chromium, cobalt, niobium, molybdenum, nickel, titanium, tungsten, vanadium, zirconium, or any other element added to obtain a desired alloying effect.
- The maximum content for any of the following elements does not exceed 1.65 wt% Mn, 0.06 wt% Si, and 0.60 wt% Cu.

In all carbon steels, small quantities of alloying elements such as Ni, Cr, and Mo are likely to be present. These elements are retained from the scrap and raw materials used in the melting process. These elements are present in minor amounts and usually have a negligible effect on the properties of the material. Carbon steels are classified into three groups according to their carbon content:

- (i) Mild steels or low-carbon steels, containing 0.08 to 0.28 wt% C
- (ii) Medium-carbon steels, containing 0.28 to 0.55 wt% C
- (iii) High-carbon steels, containing 0.55 to 1.0 wt% C

Mild steels are more resistant to aqueous corrosion and more amenable to welding and forming than those with higher C content. For these reasons, they are the most popular steels among the three classes. Carbon steel is the most widely used engineering material in the United States. Large amounts are used in nuclear and fossil power plants.

One of the two materials considered for the outer containment barrier of the Yucca Mountain repository is a low-carbon steel designated as A516 Grade 55. This wrought steel has the following composition (in wt%):

Table 3-1. Chemical composition of A516 Grade 55 steel (American Society for Testing and Materials, 1995a)

Elemental Composition (wt%)					
C	Mn	Si	P	S	Fe
<0.24 max	0.55-1.30	0.13-0.45	0.035 max	0.035 max	balance

The open literature on the oxidation of steels clearly emphasizes experimentation at higher temperatures and for much shorter times than those relevant to HLW storage containers. So care must be exercised to decide what literature can be useful for extrapolation to the conditions of interest. In this report, we are only concerned with temperatures well below 567 °C, so that wustite formation is absent.

A general qualitative discussion of the oxidation of metal-carbon alloys was published by Webb et al. (1956). Two possible reaction mechanisms were proposed. By the first mechanism, carbon from the alloy diffuses to the alloy-oxide interface, where it reacts with the scale to produce gaseous carbon oxides which may accumulate and cause the rupture of the scale. In the alternative mechanism, carbon diffuses through the scale and reacts with oxygen at the scale-gas interface. This second sequence would allow decarburization to take place without rupture.

The oxidation of binary iron-carbon (Fe-C) alloys at 500 °C was investigated by Caplan et al. (1978) and by Boggs and Kachik (1969). At 500 °C (and lower temperatures), only two oxide phases (Fe_3O_4 and Fe_2O_3) are stable. At a P_{O_2} of 0.01 atm, the oxidation rates of Fe-C alloys are much higher than that of "pure Fe" (Boggs and Kachik, 1969). At the Yucca Mountain proposed repository, P_{O_2} can vary from relatively low values up to a maximum of 0.21 atm under fully aerated conditions. At a P_{O_2} of 0.92 atm, the oxidation rate of Fe-C alloys is initially higher than that of "pure Fe" but later becomes lower as the oxidation progresses (Boggs and Kachik, 1969). After a 30 hour test, all the Fe-C alloy compositions tested (0.1 to 1 wt% C) had oxidized less than "pure Fe" (Boggs and Kachik, 1969). Parabolic scale growth was observed at steady state (after 100 minutes at a P_{O_2} of 0.92 atm, and after 1300 minutes at a P_{O_2} of 0.01 atm) and no evidence of blistering was found in the cross-sections of the scales after ~80 hours of oxidation.

The effects of the carbon content and of P_{O_2} on the oxidation rate are shown in Figures 3-1 through 3-3, which show that a carbon content of 0.1 wt% experiences its lowest initial oxidation rate at a P_{O_2} of 0.92 atm, while "pure iron" has its lowest oxidation rate at a P_{O_2} of 0.01 atm. The variation of the carbon content from 0.1 to 1 wt% did not appreciably affect the oxidation rate. An increase in P_{O_2} from 0.01 to 0.92 atm leads to a significant increase in the oxidation rate of "pure iron" but has little influence on the oxidation rate of C-containing alloys. For the oxidation of pure iron, this P_{O_2} -dependence for the initial (early) scaling rate involves a delay in the formation of hematite over magnetite, which transformation causes a sharp drop in the oxidation rate (Boggs and Kachik, 1969). The special coordinates in Figure 3-3 (that include constant terms, t_0 and W_0) provide a more accurate evaluation of the steady-state parabolic constant than does the common method of plotting the square of the weight gain as a function of time. According to Boggs and Kachik (1969), the absence of scale blistering on the surface of the Fe-C alloys results from a greater number (compared to "pure Fe") of vacancy sinks (dislocations) generated in the substrate by the precipitation of cementite during the processing of the specimen and by the subsequent volume decrease associated with decarburization. The larger number of dislocations leads to a higher vacancy annihilation capability and less tendency for vacancies to accumulate and cause local scale detachment. Consequently, the oxide scale remains in good contact with the metal substrate during the early stages of oxidation, and good contact corresponds to a maximum oxidation rate. As was shown in Figure 2-6, cold work (surface abrasion) is effective in increasing the initial oxidation rate of "pure iron" and preventing local oxide scale separation. According to Caplan and Cohen (1966), the effect of cold work prevails over the effect of annealing (as the specimens are heated for oxidation), because extra vacancy sinks are required only at the beginning when the reaction rate is the greatest and the vacancy flux a maximum.

These early interpretations concerning vacancy annihilation to support the growth of cation diffusing scales are not inconsistent with the more recent interpretations by Pieraggi and Rapp (1988), Pieraggi et al. (1995), and Hirth et al. (1995). According to these authors, cation vacancies arriving at the metal/scale interface are annihilated by the climb of both interfacial misfit dislocations in the metal and interfacial misorientation dislocations of the metal phase. The two-dimensional (2D) grid of misfit

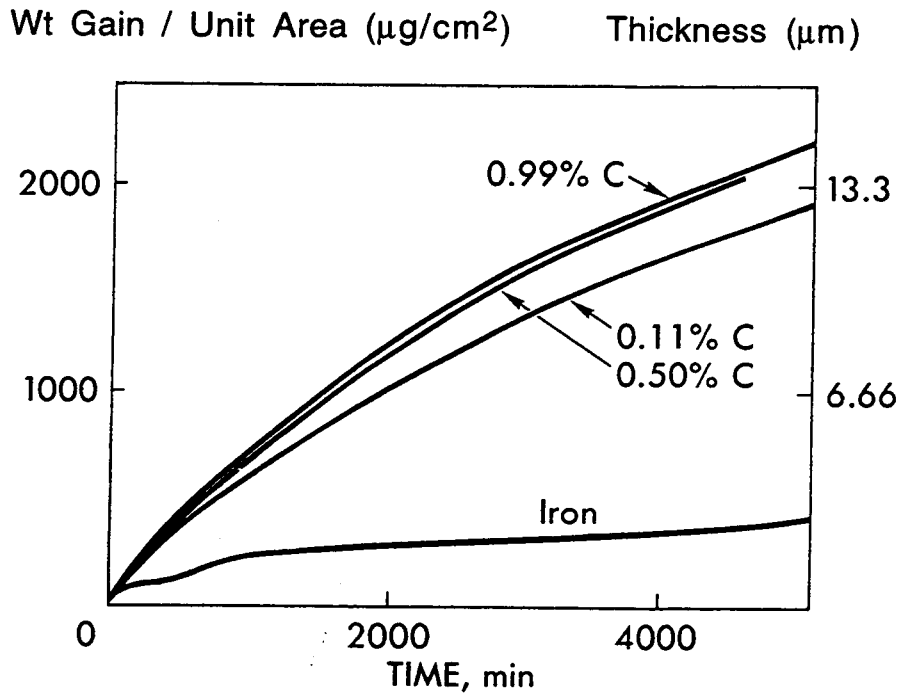


Figure 3-1. Effect of carbon concentration on the oxidation of iron-carbon alloys at 500 °C at a P_{O_2} of 0.01 atm [Boggs and Kachik (1969), reprinted with permission from The Electrochemical Society, Inc.]

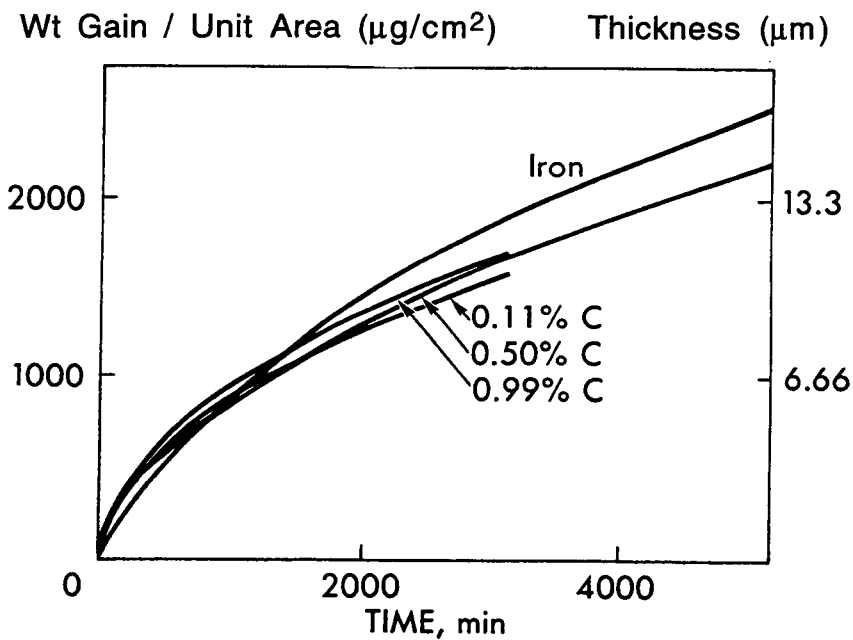


Figure 3-2. Effect of carbon concentration on the oxidation of iron-carbon alloys at 500 °C at a P_{O_2} of 0.92 atm [Boggs and Kachik (1969), reprinted with permission from The Electrochemical Society, Inc.]

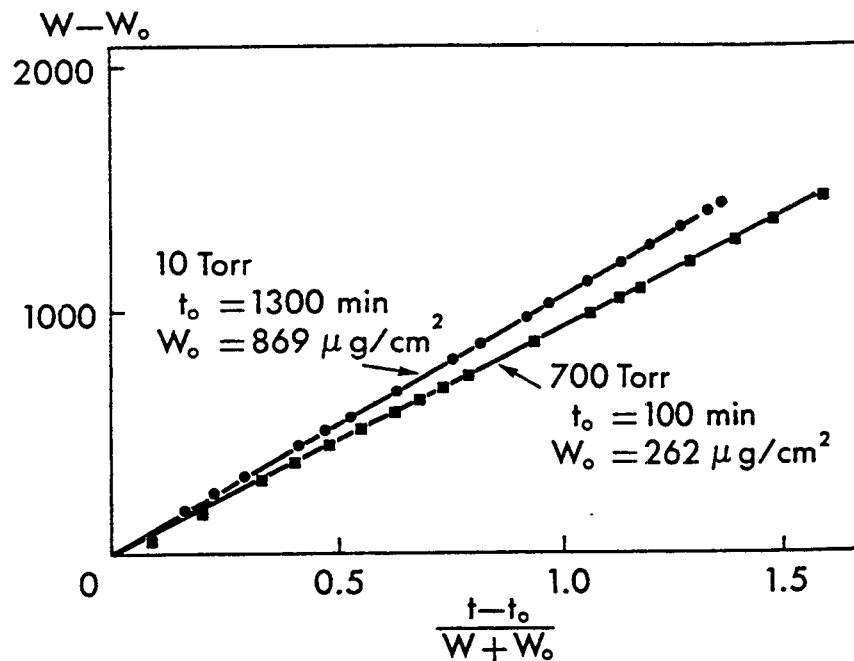


Figure 3-3. Parabolic plots for the oxidation of a Fe-1 wt% C alloy at 500 °C [Boggs and Kachik (1969), reprinted with permission from The Electrochemical Society, Inc.]

dislocations, with their Burgers vector parallel to the interface, arises from the difference in lattice constants between the metal and the scale at their epitaxial orientation, and they are inherently always present and numerous (closely spaced) for metal/oxide systems. The misorientation dislocations in the interface correspond to a minor angular tilt of the interface away from the ideal epitaxial orientation. Misorientation dislocations in the metal/scale interface can be created by either the intersection of a glide plane in the metal with the interface, or else by the passage of a screw dislocation in the metal into the oxide through the epitaxial metal/scale interface. Then the density of extrinsic (deformation) dislocations in the metal is relevant to the facility for vacancy annihilation via “interfacial” dislocation climb.

In the study of Boggs and Kachik (1969), a decarburized zone appeared at the alloy/scale interface of Fe-C alloys when they were oxidized at a P_{O_2} of 0.01 atm, but not at 0.92 atm. Their explanation for this pressure-dependence of decarburization is that pores between the oxide grains remain open to permit the escape of CO or CO_2 at an external P_{O_2} of 0.01 atm but quickly become blocked to prevent decarburization at a P_{O_2} of 0.92 atm. At the higher pressure, oxygen enters the pores faster than CO is produced, so the excess oxygen is incorporated into the oxide lattice in the pore walls. As a result, the pores close quickly at the higher oxygen pressure, blocking the escape of gaseous carbon oxides and thereby stopping further decarburization of the alloy substrate. In the study by Boggs and Kachik (1969), at a P_{O_2} of 0.92 atm. no blistering was observed.

By very long annealing of a large number of oxides, including magnetite, in ^{14}C -tagged CO/ CO_2 gases, Grabke et al. (1983) and Wolf and Grabke (1985) have shown that none of the oxides investigated has a detectable lattice solubility for carbon. Therefore, essentially no carbon can diffuse in the oxide lattice. Any carbon loss from an oxidizing steel can only occur over pores, cracks, fissures, etc. in the scale.

Coupons of the Fe-0.5 wt% C alloy were oxidized at 500 °C for 65 hours at a P_{O_2} of 0.92 atm (Boggs and Kachik, 1969); then the temperature was reduced to 350 °C and held for 2 hours. The iron diffusion rate outward through Fe_3O_4 was significantly reduced at the lower temperature. As a result, oxygen diffusing through the pores in the oxide was able to convert Fe_3O_4 into Fe_2O_3 along the pore walls. An Fe_2O_3 layer was also formed above the Fe_3O_4 layer. The new Fe_2O_3 layer, which was much more compact than the Fe_3O_4 layer, impeded the outward-bound diffusion of volatile carbon oxides. Eventually, the pores in the Fe_3O_4 layer near the interface with Fe_2O_3 became closed. This observation is in agreement with diminished decarburization at high P_{O_2} as the oxidation time progressed. From these observations, one can suppose that decarburization of carbon steels upon oxidation at the lower temperatures of the HLW containers will not occur. The flux of any volatile carbon oxides would be absolutely negligible compared to the oxygen flux from the gas phase; fissures in the oxide scale should be closed.

The effect of surface cold work (abrasion) on the oxidation of Fe-0.1 wt% C, Fe-0.5 wt% C, and Fe-1 wt% C alloys at 500 °C was investigated by Caplan et al. (1978). Some samples were chemically polished in H_2O_2 -oxalic acid, annealed at 950 °C in argon, cooled slowly to develop coarse pearlite, electropolished in perchloric-acetic acid (1:20), rinsed with dilute acetic acid and water, and blown dry. Other specimens, with cold-worked surfaces, were prepared by abrading the annealed specimens with 600-grit SiC followed by 6 μm diamond polishing, and cleaning them ultrasonically in organic solvents. The resulting oxidation curves are shown in Figure 3-4. The weight change due to carbon loss is considered to be negligible compared to the weight gain for the formation of iron oxides. The oxidation rates of the three alloys with abraded surfaces were increased by the cold working. The oxidation rate was the lowest for the annealed Fe-0.1 wt% C alloy. The faster oxidation for cold-worked samples (compared to annealed samples) can be explained by the fact that fine Fe_3O_4 grains are formed on both cold-worked pearlite and cold-worked ferrite. On annealed Fe-C alloys, pearlite oxidized faster than ferrite because the Fe_3O_4 grains are smaller when they grow over pearlite than over ferrite. As a result, annealed Fe-0.5 and Fe-1.0 wt% C alloys oxidized faster than annealed Fe-0.1 wt% C.

The time-dependences of the "instantaneous" parabolic rate constants, $k_g = 2w dw/dt$, are shown in Figure 3-5. The parabolic rate constants for oxidation of the chemically polished and annealed samples (solid lines in Figure 3-5) were time-independent. These oxidation rates of Fe-C alloys at 500 °C for a P_{O_2} of 1 atm were strongly dependent on the Fe_3O_4 grain size (Caplan et al., 1978). Fine-grain scales grew faster because the oxide grain boundaries acted as preferential diffusion paths. The oxidation rate for polycrystalline scales on Fe-C samples was ten times higher than for monocrystalline scales: k_p was $0.4 \times 10^{-10} g^2cm^{-4}s^{-1}$ for a fine-grained polycrystalline scale and $0.04 \times 10^{-10} g^2cm^{-4}s^{-1}$ for a monocrystalline Fe_3O_4 scale. Some orientations of annealed ferrite form monocrystalline Fe_3O_4 which, therefore, develop the thinnest scales. Some orientations of annealed pearlite form coarser Fe_3O_4 than others and the scale is correspondingly thinner. The external Fe_2O_3 layer is fine-grained in all cases, but it is thicker where the total scale is thin (i.e., where the Fe_3O_4 is coarse-grained) because of the lower diffusivity of Fe in the coarse-grained Fe_3O_4 . Patterns of cavities reminiscent of the prior pearlitic carbide form pearlite ghosts in the Fe_3O_4 . No decarburization occurs. Carbon cannot diffuse through the oxide lattice as elemental carbon, but only through pores in Fe_3O_4 and Fe_2O_3 as CO or CO_2 .

While the studies of Fe-C alloy oxidation by Caplan et al. (1978) and by Boggs and Kachik (1969) provide important mechanistic information, they did not provide a temperature dependence for extrapolation to lower temperatures.

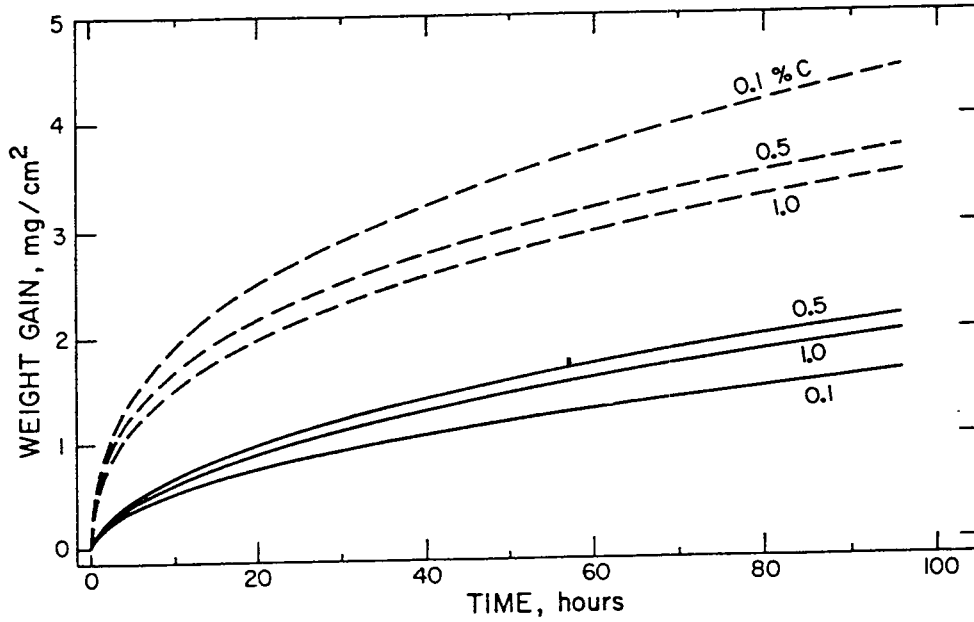


Figure 3-4. Oxidation curves for three Fe-C alloys at 500 °C. Oxidation is greater for cold-worked alloys (broken lines) than for annealed alloys (solid lines). [Caplan et al. (1978), reprinted with permission from Plenum Publishing Corporation]

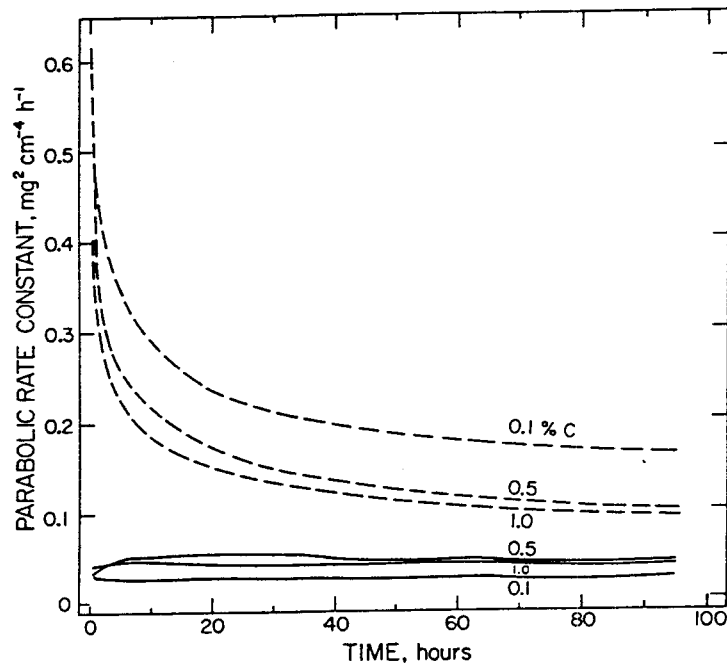


Figure 3-5. Instantaneous parabolic growth rate constants, k_p , plotted against time for Fe-C alloys oxidized at 500 °C in $P_{O_2} = 1$ atm. For cold-worked alloys (broken lines) k_p is initially very high but decreases rapidly. For annealed alloys (solid lines) k_p is smaller and relatively constant (multiply by 2.78×10^{-10} to change units from $\text{mg}^2 \text{cm}^{-4} \text{hr}^{-1}$ to $\text{g}^2 \text{cm}^{-4} \text{s}^{-1}$). [Caplan et al. (1978), reprinted with permission from Plenum Publishing Corporation]

The oxidation of Fe-C alloys at a P_{O_2} of 0.13 atm and temperatures in the range 200–350 °C was investigated by Runk and Kim (1970). High-purity carbon steels of 0.2, 0.4, and 0.8 wt% C were studied. The surfaces of the samples were ground with 600 grit SiC paper. The time-dependence of the weight gains at 350 °C is shown in Figures 3-6 and 3-7. The samples all had a fine pearlitic microstructure. A two-stage logarithmic law was observed in Figure 3-6 up to an oxidation time of about 35 minutes.¹ For longer periods of time, a parabolic rate law was observed up to about 100 minutes, after which a slight negative deviation (slower oxidation) from the parabolic behavior occurred. This negative deviation was also observed for the oxidation of iron at 350 °C for oxygen partial pressures ranging from 0.001 to 0.13 atm (Boggs et al., 1965; 1967). They also reported an initial parabolic growth period during which only Fe_3O_4 was formed, followed by a second but slower parabolic growth rate during which $\alpha-Fe_2O_3$ was also present. They credited the retardation effect of $\alpha-Fe_2O_3$ to an abrupt decrease in the thermodynamic activity of oxygen available at the outer interface of Fe_3O_4 . At 220 °C and 0.01 atm of oxygen, they observed only the formation of Fe_3O_4 during a 150-minute oxidation test.

The experiments of Runk and Kim showed that the oxidation rate increased with increasing carbon content from 0.2 to 0.8 wt% C. The rate constants k_1 and k_2 , for the two logarithmic regions, and k_g , for the parabolic region are given in Table 3-2, where k_1 and k_2 are the values published by Runk and Kim (1970). The k_g values were recalculated by the method suggested by Pieraggi (1987), which consists in plotting the weight gain as a function of the square root of time, instead of the traditional plot of $(\Delta m/A)^2$ versus time. The Pieraggi method provides a more accurate value of a steady-state k_g than the common method used by Runk and Kim.

Table 3-2. Oxidation rate constants at 350 °C and at a P_{O_2} of 0.13 atm for Fe-C alloys with fine pearlite and various carbon contents (Runk and Kim, 1970)

Rate Constant	0.2 wt% C	0.4 wt% C	0.8 wt% C
k_1 (mg/cm ²)	1.02×10^{-3}	1.13×10^{-3}	1.17×10^{-3}
k_2 (mg/cm ²)	1.83×10^{-3}	2.00×10^{-3}	2.60×10^{-3}
k_g (mg ² /cm ⁴ yr)	0.123	0.155	0.373

From the parabolic rate constants listed in Table 3-2, the mass gain per unit area, thickness of the oxide scale, and metal recession depth for a period of 1,000 years of oxidation at 350 °C were calculated and are listed in Table 3-3. The conversion equations used for these calculations are presented in the next section.

Carbon steels with various microstructures were studied to investigate the influence of the ferrite-carbide phase boundary on the oxidation rate of Fe-0.8 wt% C alloys (Runk and Kim, 1970). Three types of microstructure were studied: fine pearlitic, coarse pearlitic, and spheroidized carbide phase. The samples

¹ In fact, the data in the original Figures 1 through 4 of Runk and Kim (Figures 3-6 through 3-9 of this report) state a 300 °C oxidation temperature, but their data indeed correspond to a 350 °C temperature for internal consistency.

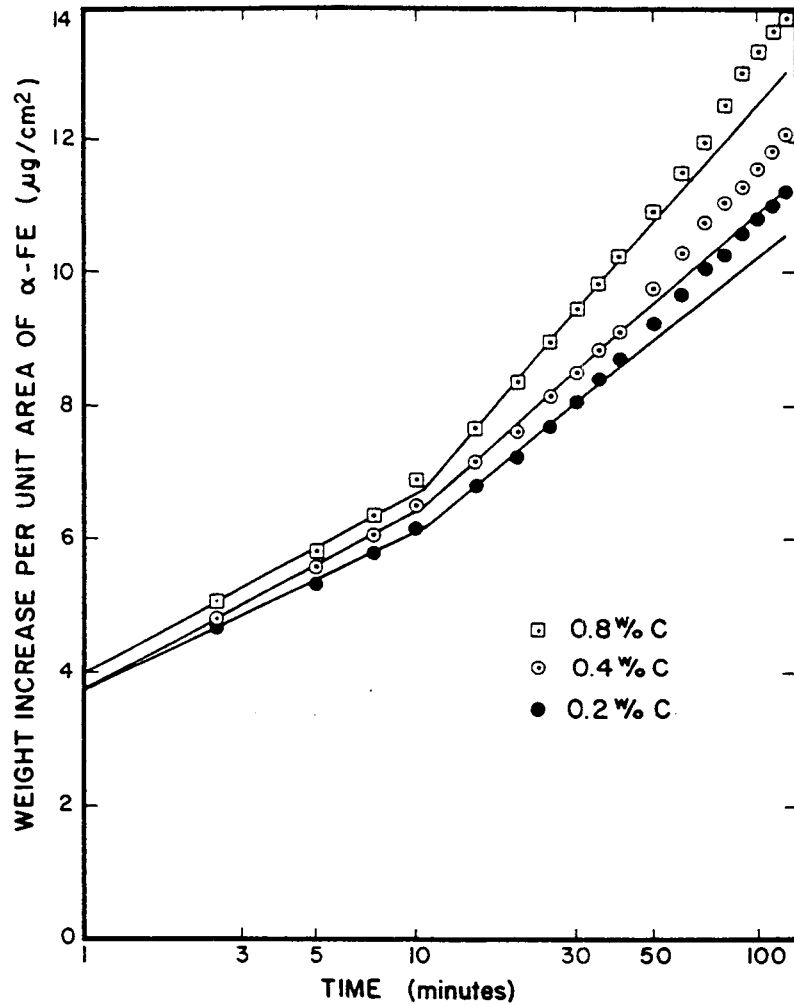


Figure 3-6. Semi-logarithmic plots of oxidation of pearlitic carbon steels containing various amounts of carbon at a temperature of 350 °C and oxygen partial pressure of 0.13 atm [Runk and Kim (1970), reprinted with permission from Plenum Publishing Corporation]

were oxidized at 350 °C at a P_{O_2} of 0.13 atm. Again, a two-stage logarithmic dependence was followed by parabolic behavior, as shown in Figures 3-8 and 3-9. A negative deviation from parabolic behavior occurred at times longer than 100 minutes for the two pearlite structures, but not for the alloy containing the spheroidized carbide (although such deviation might appear after a longer oxidation period, since the experiments lasted only 120 minutes). The oxidation rate was found to increase with increasing ferrite-carbide phase boundary length (all the samples had the same true lamellar spacing: $\sim 2.0 \mu\text{m}$). The phase boundary length is proportional to the inverse of the carbide lamellar width for the pearlitic microstructures, and to the inverse of the carbide sphere radius for the spheroidized microstructure. The rate constants for the three regions are given for each microstructure in Table 3-4. For the practical application of the steel HLW container, the early linear rates are unimportant, and the parabolic rates need to be extrapolated to very much longer times, as presented in Table 3-5.

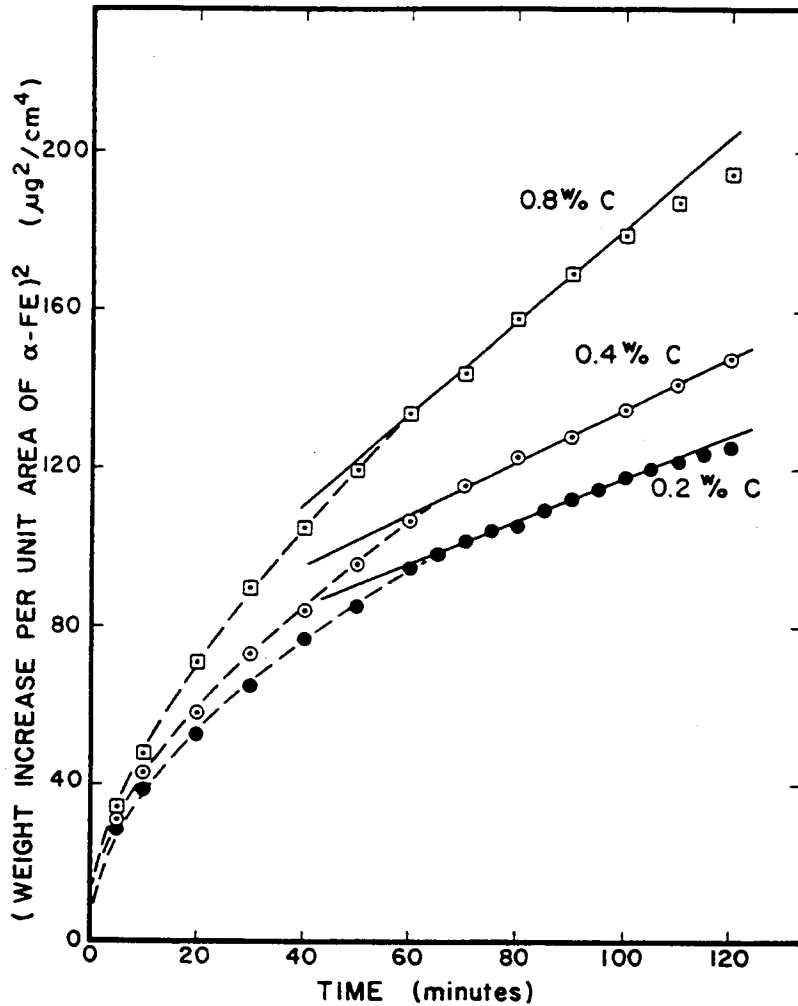


Figure 3-7. Parabolic plots of oxidation of pearlitic carbon steels containing various amounts of carbon at a temperature of 350 °C and oxygen partial pressure of 0.13 atm (replotted from the data of Runk and Kim, 1970)

The temperature-dependence of the low temperature oxidation of a Fe-0.8 wt% C alloy was investigated (Runk and Kim, 1970). The specimens were polished (abraded) with "Linde A" to ensure a uniform surface roughness so that a more accurate oxide thickness could be estimated from the weight gain measurement. Weight changes were recorded at 200, 250, 300, and 350 °C on samples with a fine pearlitic microstructure. The initial two-stage logarithmic kinetics steps were observed at all temperatures, as seen in Figure 3-10, but these have negligible importance for oxidation during long term service. The time spans covered by these two regimes increased with decreasing temperature. A parabolic regime was established for longer oxidation times at temperatures of 250, 300, and 350 °C, as shown in Figures 3-11 and 3-12. At 200 °C, logarithmic behavior was maintained for 200 minutes (the entire duration of the experiment), as was also observed for the oxidation of iron below 200 °C (Vernon et al., 1953). The data published by Runk and Kim (1970), after recalculation by the Pieraggi method, were used to calculate the temperature dependence of the gravimetric parabolic rate constant k_g for the oxidation of Fe-0.8 wt% C alloys with fine pearlitic microstructure:

Table 3-3. Mass gain ($\Delta m/A$), thickness of the oxide scale (X), and recession thickness (R) calculated for a period of 1,000 years of oxidation of Fe-C alloys with fine pearlite at 350 °C and at a P_{O_2} of 0.13 atm

Progress of Oxidation	0.2 wt% C	0.4 wt% C	0.8 wt% C
$\Delta m/A$ (mg/cm ²)	11.1	12.4	19.3
X (μm)	76	86	132
R (μm)	36	41	63

$$\log k_g \text{ (mg}^2/\text{cm}^4\text{yr)} = 9.515 - 6,190/T \quad (3-1)$$

where T is in °K. From this expression, the mass gain per unit area, thickness of the oxide scale, and recession thickness for a period of 1,000 years of oxidation were calculated and are listed in Table 3-6. The values in parentheses correspond to an Fe-0.2 wt% C alloy with fine pearlite, as inferred from the rates given in Table 3-2. As shown in Table 3-5, a more coarse carbide morphology would provide lower values, and use of a chemical etching surface preparation to replace surface grinding would provide yet slower kinetics.

Electron microscopy observations by Runk and Kim (1970) showed that the oxides initially formed on both the ferrite and the carbide phases were each relatively uniform, with an average grain size less than 100 Å. The oxide formed over the carbide lamellae was thinner than that formed over the ferrite phase. A similar morphology was observed over samples with spheroidized carbide oxidized for 10 minutes.

After the pearlitic steel was oxidized for 20 minutes at 300 °C, the oxide over the ferrite phase was thicker than that over the carbide phase. At that time, raised ridges began to appear near the ferrite-carbide grain boundaries. From that time on, the phase boundary lines became less evident, indicating that the oxide over the ferrite had begun to overgrow the carbide area. An x-ray analysis indicated that the oxide film formed over the ferrite was either Fe_3O_4 or $\gamma\text{-Fe}_2\text{O}_3$, most likely the former (Kofstad, 1988). The average oxide grain size was determined to be 200 Å.

As the oxidation of the pearlitic steel at 300 °C progressed for longer times (70 minutes), the oxide phase over the ferrite phase spread more extensively over the carbide area. At this point, x-ray diffraction clearly showed that the oxide phase was Fe_3O_4 , with a median crystallite size of 300 Å. After 120 minutes, the spreading of the oxide phase over the ferrite area to the carbide area was even more extensive. Some $\alpha\text{-Fe}_2\text{O}_3$ started to be detected within the major Fe_3O_4 phase. The appearance of the new phase correlates to the negative deviation from the parabolic rate (Figures 3-7 and 3-9). The mean crystallite size remained unchanged.

Since the oxide formed over the carbide phase was observed to be thin and protective, the measured weight gain per unit area of the coupon was assumed to represent the kinetics of oxide growth over the ferrite phase (Runk and Kim, 1970). This interpretation of the initial kinetics is also based on the observation that Fe_3O_4 is the only oxide formed initially. The parabolic rates of oxide growth at

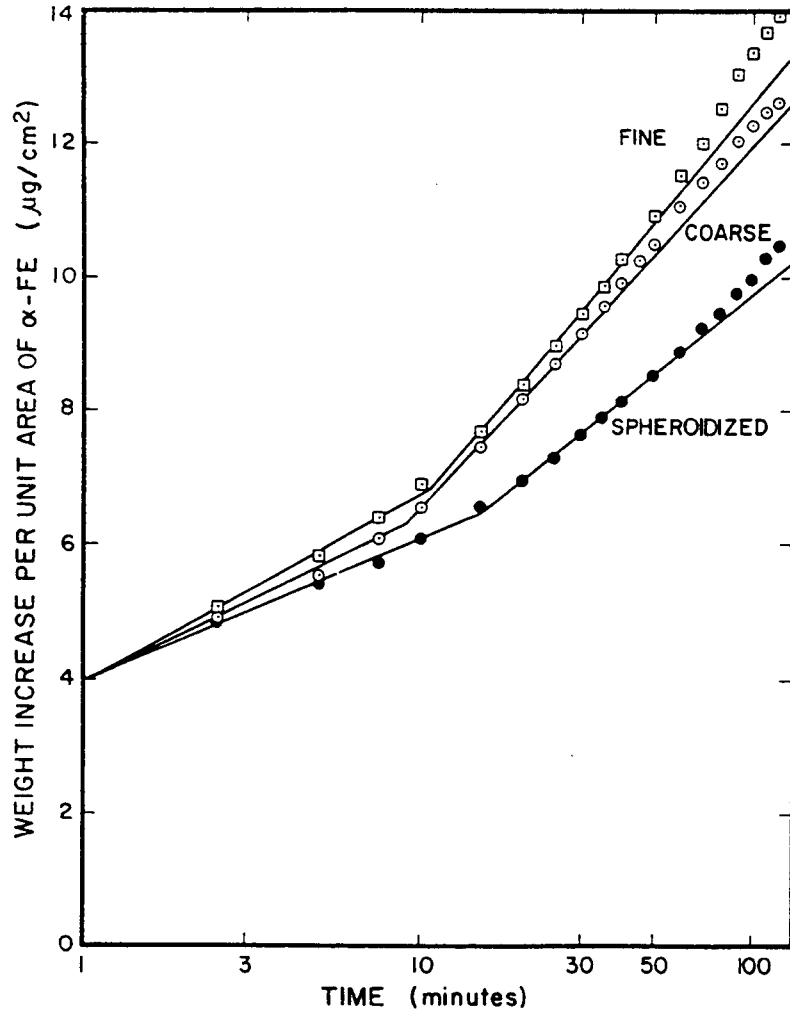


Figure 3-8. Logarithmic plots of oxidation of pearlitic carbon steels containing 0.8 wt% carbon and having three distinct microstructures (fine pearlite, coarse pearlite, and spheroidite) at 350 °C under an oxygen partial pressure of 0.13 atm [Runk and Kim (1970), reprinted with permission from Plenum Publishing Corporation]

temperatures ranging from 250 to 350 °C can be interpreted by the theory for diffusion-controlled, parabolic scaling (Wagner, 1951). Because the activation energy observed during the parabolic growth of oxide (51 kJ/mol) is smaller than the values reported for lattice diffusion in Fe_3O_4 (230 kJ/mol, Himmel et al., 1953; 350 kJ/mol, Klotsman et al., 1960; 140 kJ/mol, Dieckmann and Schmalzried, 1977), the growth of the magnetite scale is attributed to diffusion of Fe ions along the grain boundaries. Obviously, a grain boundary diffusion mechanism also has a larger parabolic rate constant than a lattice diffusion mechanism (McLean, 1957; Perrow et al., 1968). The extrapolation of Paidassi's (1958) high temperature data for Fe_3O_4 growth controlled by lattice diffusion to 300 °C gives a gravimetric constant (k_g) value of $7.8 \times 10^{-4} \text{ mg}^2/\text{cm}^4\text{min}$. In comparison, the value of $0.11 \text{ mg}^2/\text{cm}^4\text{min}$ obtained from the measurements by Runk and Kim (1970) is much higher, which is another indication that grain boundary diffusion of Fe ions is the dominant process at this low temperature.

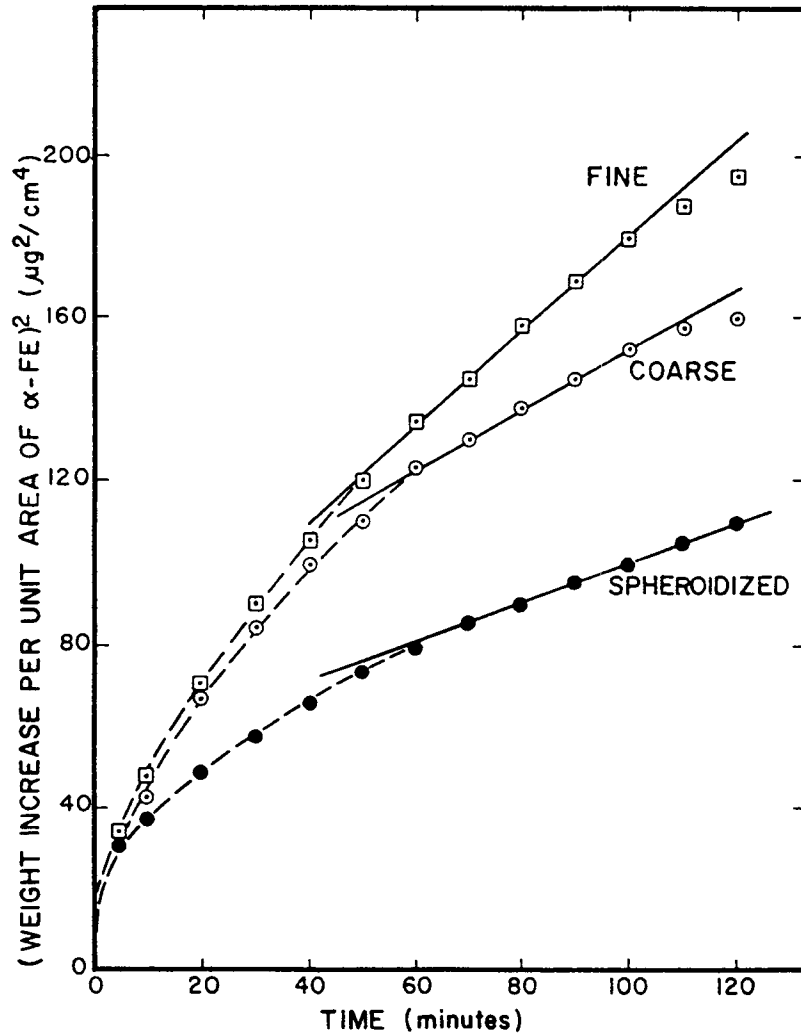


Figure 3-9. Parabolic plots of oxidation of pearlitic carbon steels containing 0.8 wt% carbon and having three distinct microstructures (fine pearlite, coarse pearlite, and spheroidite) at 350 °C under an oxygen partial pressure of 0.13 atm [Runk and Kim (1970), reprinted with permission from Plenum Publishing Corporation]

The variation of the oxidation rate at 300 °C as a function of the relative phase boundary length is shown in Figure 3-13. During the initial logarithmic stage, the phase boundary length has very little or no effect on the reaction rate constant. During the second logarithmic stage (that starts after 10 minutes of oxidation), on the other hand, the reaction rate clearly increased linearly with the increase in phase boundary length. The number of large crystallites that form during this stage (and grow from the ferrite area into the carbide area) is proportional to this boundary length. The phase boundary effect was expressed mathematically by Runk and Kim. A logarithmic kinetics expression for a single crystal specimen of pure iron is written in terms of the oxygen weight gain (W):

Table 3-4. Oxidation rate constants at 350 °C at a P_{O_2} of 0.13 atm for Fe-0.8 wt% C alloys with various microstructures (Runk and Kim, 1970). Values in parentheses correspond to Fe-0.2 wt% C alloy.

Rate Constant	Fine Pearlite	Coarse Pearlite	Spheroidized C
k_1 (mg/cm ²)	1.17×10^{-3}	1.02×10^{-3}	0.90×10^{-3}
k_2 (mg/cm ²)	2.60×10^{-3}	2.35×10^{-3}	1.71×10^{-3}
k_g (mg ² /cm ⁴ yr)	0.373 (0.123)	0.167 (0.055)	0.117 (0.039)

Table 3-5. Mass gain ($\Delta m/A$), thickness of the oxide scale (X), and recession depth (R) calculated for a period of 1,000 years of oxidation of Fe-0.8 wt% C at 350 °C at a P_{O_2} of 0.13 atm. Values in parentheses correspond to Fe-0.2 wt% C alloy.

Progress of Oxidation	Fine Pearlite	Coarse Pearlite	Spheroidized C
$\Delta m/A$ (mg/cm ²)	19.3 (11.1)	12.9 (7.4)	10.8 (6.2)
X (μm)	132 (76)	88 (50)	73 (42)
R (μm)	63 (36)	42 (24)	35 (20)

Table 3-6. Mass gain ($\Delta m/A$), thickness of the oxide scale (X), and recession thickness (R) calculated for Fe-0.8 wt% C with fine pearlite for a period of 1,000 years in 0.13 atm of dry oxygen. Values in parentheses correspond to Fe-0.2 wt% C alloy.

Temperature (°C)	$\Delta m/A$ (mg/cm ²)	X (μm)	R (μm)
300	7.2 (4.1)	50 (29)	24 (14)
275	4.1 (2.4)	28 (16)	13 (7)
250	2.2 (1.3)	15 (9)	7.2 (4.1)
225	1.1 (0.6)	7.6 (4.4)	3.6 (2.1)
200	0.52 (0.30)	3.6 (2.1)	1.7 (1.0)

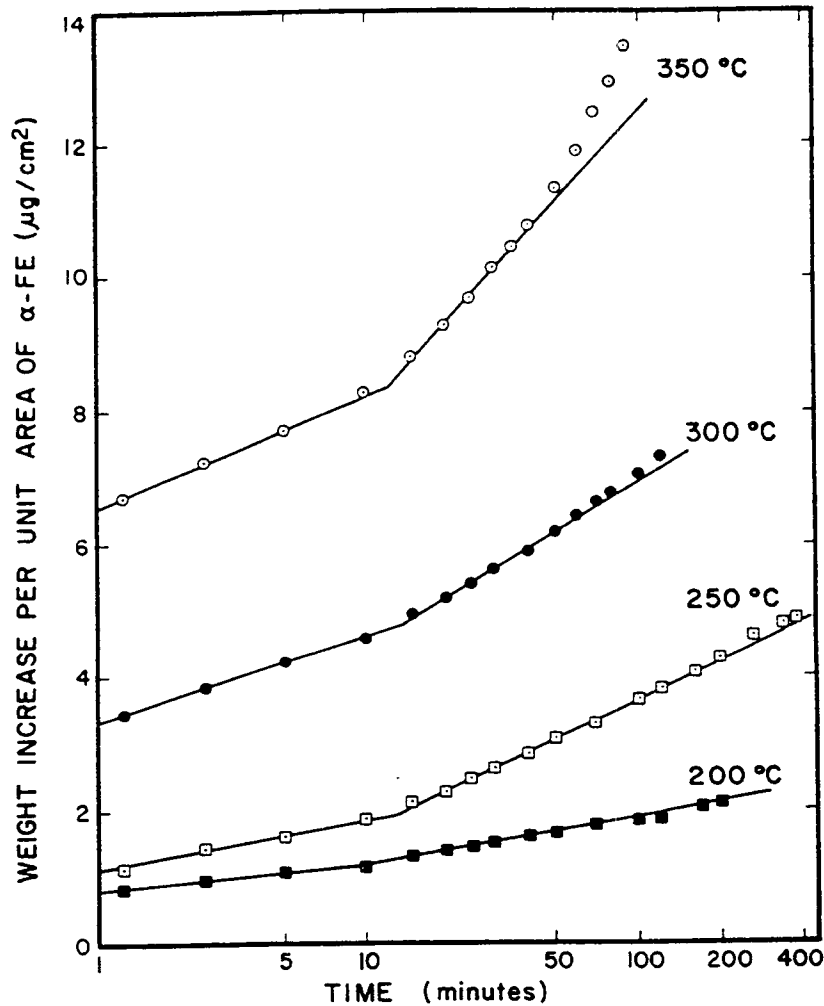


Figure 3-10. Logarithmic plots showing the influence of temperature on the oxidation rate of a pearlitic carbon steel containing 0.8 wt% carbon at an oxygen partial pressure of 0.13 atm [Runk and Kim (1970), reprinted with permission from Plenum Publishing Corporation]

$$W = k^{\circ} [\ln(t/\tau) + 1] \quad (3-2)$$

where k° is the rate constant for pure iron (without phase boundaries) and τ is a time constant. A corresponding equation for the weight gain obtained from a sample with ferrite/carbide phase boundaries is expressed as:

$$W + Wb = k [\ln(t/\tau) + 1] \quad (3-3)$$

where k is the rate constant for a carbon steel with grain boundaries, and Wb is the additional weight gain due to the phase boundaries, where b is a linear function of the phase boundary length. The rearrangement of Eq. (3-3) gives:

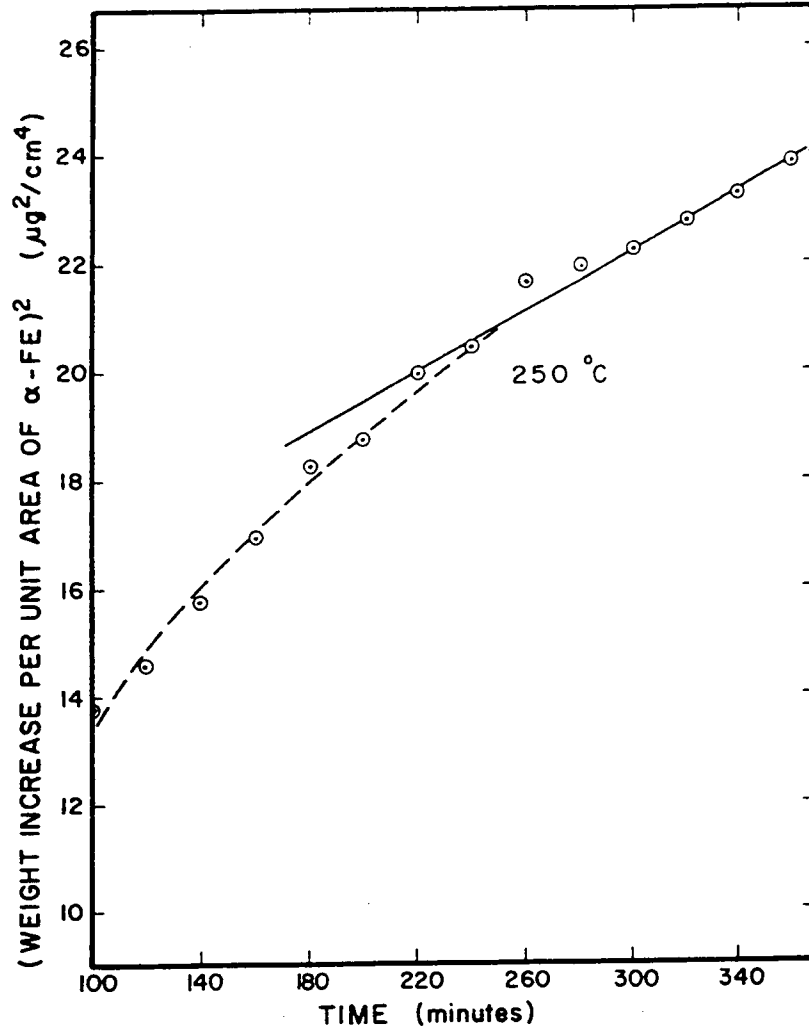


Figure 3-11. Parabolic plot of oxidation of a pearlitic carbon steel containing 0.8 wt% carbon oxidized at 250 °C under an oxygen partial pressure of 0.13 atm [Runk and Kim (1970), reprinted with permission from Plenum Publishing Corporation]

$$W = [k/(1 + b)] [\ln(t/\tau) + 1] \quad (3-4)$$

which can be combined with Eq. (3-2) to give:

$$k/k^{\circ} = 1 + b \quad (3-5)$$

This indicates that the logarithmic rate constant increases linearly with the boundary length. A similar equation is obtained for the parabolic rate constant:

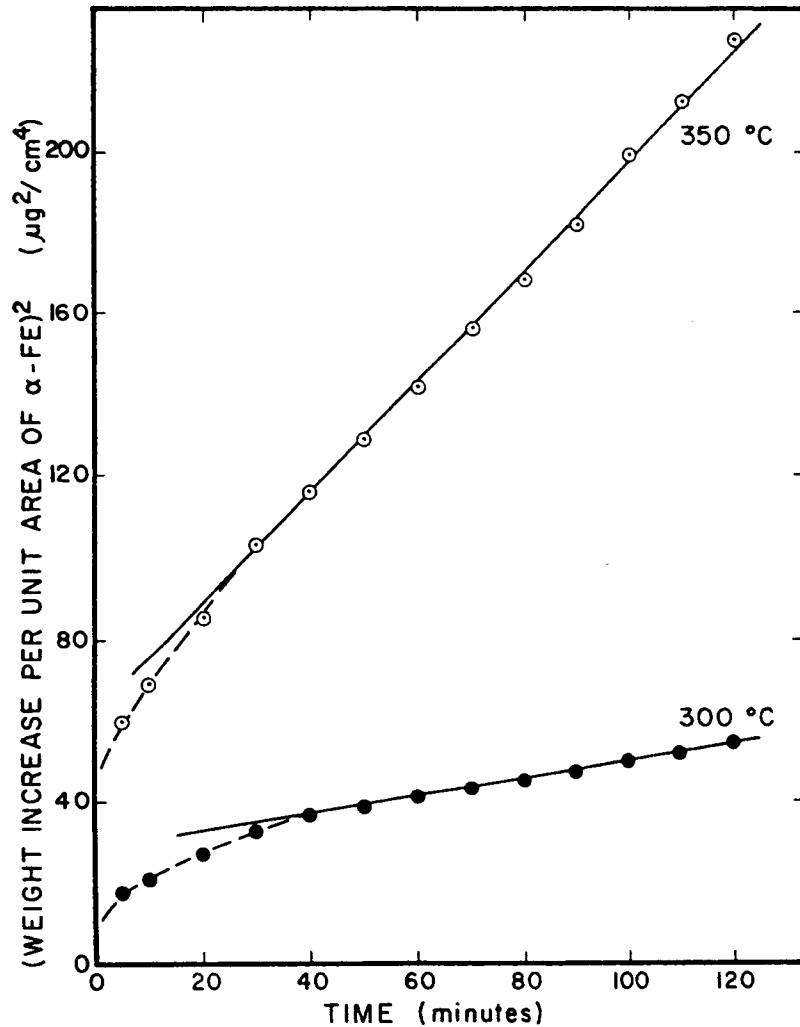


Figure 3-12. Parabolic plot of oxidation of pearlitic carbon steels containing 0.8 wt% carbon oxidized at 300 and 350 °C under an oxygen partial pressure of 0.13 atm [Runk and Kim (1970), reprinted with permission from Plenum Publishing Corporation]

$$kg/kg^{\circ} = (1 + b)^2 \quad (3-6)$$

This expression indicates that the parabolic rate constant is also dependent on the boundary length.

In summary, to minimize the scaling kinetics for a steel with a given composition, the metal should be fully annealed to achieve spheroidization of the carbide, and to remove the cold work which supports vacancy annihilation at the metal-scale interface. A chemical preparation of the surface (etching/polishing) is preferred to a mechanical polishing, grinding or grit blasting for the same reason.

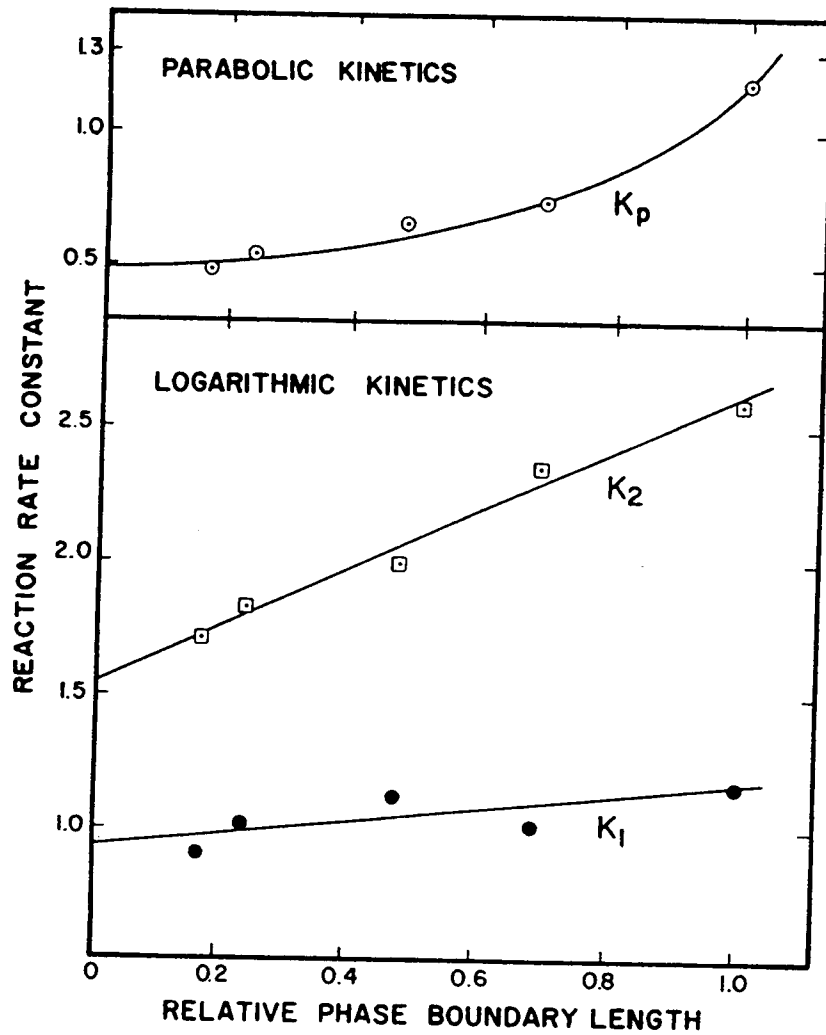


Figure 3-13. Influence of phase boundary length on the oxidation rate at 300 °C for two-phase, Fe-Fe₃C substrate of Fe-0.8 wt% C with fine pearlite morphology. The dimensions on k_1 and k_2 are mg/cm². The dimensions of k_p are mg²/cm⁴min. [Runk and Kim (1970), reprinted with permission from Plenum Publishing Corporation]

4 OXIDATION OF Fe-2.25Cr-1Mo IN DRY AIR AND OXYGEN

A steel is considered to be an "alloy steel" when the maximum of the range given for the content of alloying elements exceeds one or more of the following limits (Craig, 1989): (a) 1.65 wt% Mn, (b) 0.60 wt% Si, and (c) 0.60 wt% Cu. A steel is also considered to be an alloy steel when a definite quantity of the following elements is specified or required within the limits of the recognized constructional alloy steels: Al, Cr, Co, Mo, Ni, Nb, Ti, W, V, Zr, or any other element added to obtain a specified alloying effect. As a rule, the total amount of alloy in the AISI-SAE grades designated as "alloy steels" does not exceed approximately 4.0 wt% above that permitted in carbon steels. Therefore, the degree of alloying of "alloy steels" is in between those for "carbon steels" and "stainless steels." "Low-alloy steels" contain approximately 5 wt% or less total alloying. In environments that are not too corrosive (e.g., rural or desert environment, such as the Yucca Mountain site) small additives of Cu, P, Cr, and Ni in alloy steels provide significant improvement in atmospheric (ambient temperature) corrosion resistance compared to carbon steels (Craig, 1989).

Low-alloy steels containing 0.5 to 1 wt% Mo and 0.5% to 9% Cr have mechanical properties that are distinctly superior to those of carbon steels (Craig, 1989; Davis, 1996). The steel containing 1% Mo and 2.25% Cr, referred to as Fe-2.25Cr-1Mo, has especially high creep strength, yield strength, tensile strength, and oxidation resistance (Davis, 1996). Since creep of low-alloy steels has been observed only at temperatures above ~370 °C (Davis, 1996), its long-term effect on the mechanical integrity of Fe-2.25Cr-1Mo containers held at temperatures in the range 100–300 °C should be minimal. Moreover, Fe-2.25Cr-1Mo has an excellent service record in both fossil-fuel and nuclear-fuel plants. This steel is a candidate material for the outer HLW container. The steel, also designated as A387 Grade 22, has the following composition (in wt%):

Table 4-1. Chemical composition of A387 Grade 22 steel (American Society for Testing and Materials, 1995b)

Elemental Composition (wt%)					
C	Mn	Si	Cr	Mo	Fe
<0.17	0.25–0.66	0.5 max	1.88–2.62	0.85–1.15	balance

In dilute Fe-Cr alloys, the low-temperature limit for wustite stability is somewhat higher than for pure Fe (Yearian et al., 1956; Douglass et al., 1986). Molybdenum also has the effect of shifting the formation of wustite to higher temperatures (Rahmel, 1961). These low-alloy steels contain chromium and molybdenum primarily to improve their mechanical properties by the formation of dispersed stable carbides. They have been used extensively for the manufacture of boiler tubes, water walls, and furnace components for pulverized coal combustion plants for temperatures up to 600 °C.

The Cr and Mo alloying elements also permit the use of these steels in high-pressure hydrogen at intermediate temperatures, as shown in the "Nelson diagram" of Figure 4-1 (Prescott, 1980). The Nelson diagram plots the steel compositions providing one year service life in pressurized hydrogen as a function of temperature. The favorable action of the alloying elements in this environment results from the higher thermodynamic stabilities of their carbides, which resist reaction with interstitial hydrogen to form methane bubbles at the ferrite grain boundaries (Shewmon, 1976; Sundarajan and Shewmon, 1981).

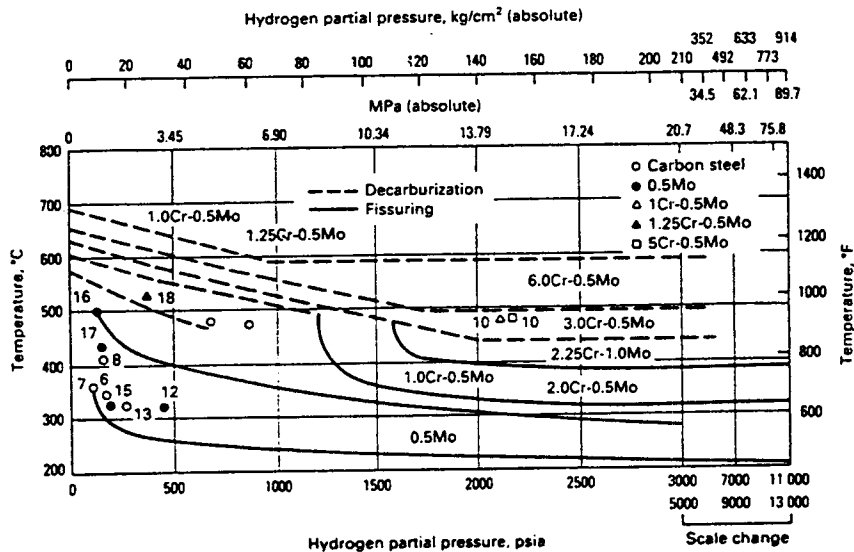


Figure 4-1. Nelson diagram for operating limits of steels in pressurized hydrogen in one-year service. Failure by hydrogen attack occurs after one year above the lines. This diagram displays the superior resistance to hydrogen attack of steels containing Cr and Mo (Prescott, 1980).

The segregation of elements in iron-(transition metal) alloys has been reported (Holmes et al., 1974; Tomlinson et al., 1978; Khanna and Singh, 1982; Khanna and Gnanamoorthy, 1982; McMahon, 1968; Rellick and McMahon, 1974; Ohtani and McMahon, 1975; Ucisik et al., 1978; Murza and McMahon, 1980; Yu and McMahon, 1980a; Yu and McMahon, 1980b; Takayama et al., 1980; Misra and Rao, 1992; Mackenbrock and Grabke, 1992; Mintz et al., 1992). The segregation of elements such as P and S can lead to embrittlement, but no mention of promotion of enhanced grain boundary oxidation due to these elements was found in the literature.

The oxidation of Fe-2.25Cr-1Mo steel in dry oxygen at 550–700 °C was studied by Simms and Little (1987). The oxidation product was a multilayer scale comprising a doped inner magnetite layer, a central magnetite layer, and an outer hematite layer. Examination by the x-ray diffraction technique indicated that the magnetite layers were possibly in slight tension. The morphology is similar to those obtained on pure Fe and low-Cr alloys (Simms and Little, 1987; Hussey et al., 1977). The elements added to the alloy for increased strength are partitioned between each of these oxide layers in a manner that can be explained by a combination of diffusion theory and the preference of certain metallic ions for either octahedral or tetrahedral sites in the growing oxide layer (Simms and Little, 1987). The diffusivities of Fe^{3+} and Mn^{2+} (present as an impurity) in spinel oxides are much higher than the diffusivity of Cr^{3+} . This fact corresponds well to the observation that Cr segregates to the inner spinel layer, while Mn is spread through both the inner and outer layers of the spinel. The activation energy for the global parabolic (gravimetric) oxidation of Fe-2.25Cr-1Mo is ~ 170 kJ/mol, correlating well with similar results on low-Cr alloy steels, as well as the activation energy found for pure iron oxidation. The gravimetric parabolic rate constant, k_g , is defined as:

$$(\Delta m/A)^2 = k_g t \quad (4-1)$$

where $(\Delta m/A)$ and t are the mass gain per unit area and time, respectively. The recession rate constant, k_r , defined by

$$R^2 = k_r t \quad (4-2)$$

expresses the rate at which the metal surface is consumed (recedes) to form an oxide. The practical scaling rate constant, k_p , describes the thickness of the oxide formed, and is defined by

$$X^2 = k_p t \quad (4-3)$$

These relations have also been used in the preceding chapter to calculate the values reported in Tables 3-3, 3-5, and 3-6.

The micrograph published by Simms and Little (1987) for Fe-2.25Cr-1Mo, shown in Figure 4-2, indicates that the sum of the thicknesses of the two magnetite layers formed at 600 °C is approximately six times the thickness of the hematite layer. From this observation, the average oxide molecular weight M_{FeO_x} of the oxide scale can be estimated as:

$$M_{FeO_x} = \left(\frac{6(1/3)(M_{Fe_3O_4}) + (1/2)(M_{Fe_2O_3})}{7} \right) \quad (4-4)$$

which gives:

$$M_{FeO_x} = 77.56 \text{ g/mole Fe} \quad (4-5)$$

The average density ρ_{FeO_x} for the two-layered scale is calculated by an expression analogous to Eq. (4-4) to give

$$\rho_{FeO_x} = 5.19 \text{ g/cm}^3 \quad (4-6)$$

Then the parabolic recession rate constant is calculated by the expression:

$$k_r \left(\frac{\text{cm}^2}{\text{yr}} \right) = k_g \left(\frac{\text{g oxygen}}{\text{cm}^4 \cdot \text{yr}} \right)^2 \left[\left(\frac{55.85 \text{ g Fe}}{21.71 \text{ g O}} \right) \left(\frac{\text{cm}^3}{7.86 \text{ g Fe}} \right) \right]^2 \quad (4-7a)$$

or

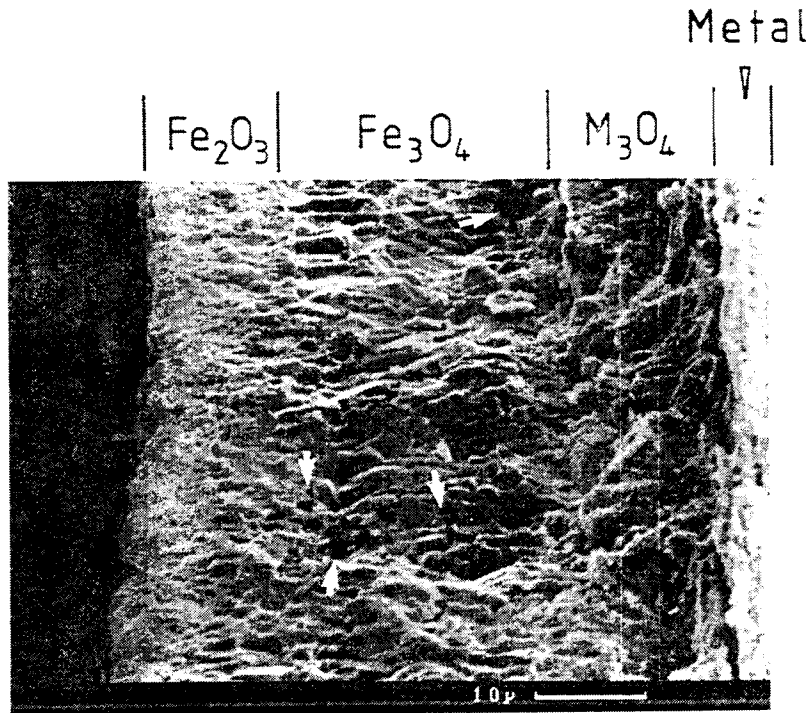


Figure 4-2. Micrograph showing the various layers of oxidized Fe-2.25Cr-1Mo (Simms and Little, 1987). The micrograph indicates that the sum of the thicknesses of the two magnetite layers formed at 600 °C is approximately six times the thickness of the hematite layer.

$$k_r \left(\frac{cm^2}{yr} \right) = 0.1071 k_g \left(\frac{(g \text{ oxygen})^2}{cm^4 \cdot yr} \right) \quad (4-7b)$$

or

$$k_r \left(\frac{cm^2}{yr} \right) = 1.071 \times 10^{-7} k_g \left(\frac{(mg \text{ oxygen})^2}{cm^4 \cdot yr} \right) \quad (4-7c)$$

The parabolic practical rate constant is easily calculated from the parabolic recession rate constant:

$$k_p \left(\frac{cm^2 FeO_x}{yr} \right) = \left[k_r \left(\frac{cm^2 Fe}{yr} \right) \right] \left(\frac{V_{FeO_x}}{V_{Fe}} \right)^2 \quad (4-8a)$$

where V_{FeO_x} and V_{Fe} are the average molar volumes of the two-layer oxide scale and of iron, respectively. For $V_{FeO_x} = 14.94 \text{ cm}^3/\text{mol}$ and $V_{Fe} = 7.11 \text{ cm}^3/\text{mol}$, then

$$k_p \left(\frac{\text{cm}^2 \text{FeO}_x}{\text{yr}} \right) = 4.423 k_r \quad (4-8b)$$

These three parabolic rate constants are plotted on alternate ordinate scales in Figure 4-3, and are tabulated for temperatures of interest in Table 4-2. Significant porosity is observed in the oxide scale of the Fe-2.25Cr-1Mo steel, especially in the magnetite layer at the higher temperature of the investigated range. This porosity could act as crack nucleation sites, leading to the mechanical failure of the oxides, which might also permit penetration of the scale by the oxidizing gas. For this reason, secondary oxidant components in the environment, such as carbon, sulfur and nitrogen, are often found in steels beneath the scale, although these elements are virtually insoluble in the scale. The average alloy grain size from this study (which is an important parameter, as explained later) was $\sim 40 \mu\text{m}$ as observed on the micrographs.

Table 4-2. Parabolic rate constants and estimated breakaway times calculated with the data of Simms and Little (1987) obtained in dry oxygen in the temperature range 550–700 °C. The breakaway is assumed to occur when the surface weight gain reaches 12 mg/cm² (see Figure 4-4).

T (°C)	log k_p (mg ² /cm ⁴ yr)	log k_r (cm ² /yr)	log k_p (cm ² /yr)	Breakaway Time (yr)
300	-1.873	-8.843	-8.197	10,700
275	-2.590	-9.561	-8.915	56,100
250	-3.377	-10.347	-9.701	343,000
225	-4.242	-11.212	-10.566	2,510,000
200	-5.199	-12.169	-11.523	22,800,000
175	-6.262	-13.232	-12.587	263,000,000
150	-7.451	-14.421	-13.776	4,070,000,000
125	-8.790	-15.760	-15.114	88,700,000,000
100	-10.307	-17.277	-16.632	2.92×10^{12}

The corners and edges of coupons are the preferred sites for mechanical fracture as the outward growing oxide thickens to achieve sufficient strength to detach from the shrinking metal core. If the molecular oxidant can pass over the pores, then it will bypass solid-state diffusion. The associated accelerated kinetics are called "breakaway," and they represent the end of the protective parabolic behavior. Thus, the rate constants given in Figure 4-3 and Table 4-2 can be used to calculate the minimum extent of reaction for a given time. The initiation of breakaway oxidation should be expected to depend upon substrate geometry, with a convex substrate worse than a flat or concave substrate. Breakaway times for planar geometry were calculated and included in Table 4-2. These times were calculated on the assumption that the oxide scale spalls when the oxide layer reaches a thickness such that the surface

$$k_g: y = 13.864 + -9019.5x \quad R = 0.99968$$

$$k_r: y = 6.8935 + -9019.5x \quad R = 0.99968$$

$$k_p: y = 7.5392 + -9019.5x \quad R = 0.99968$$

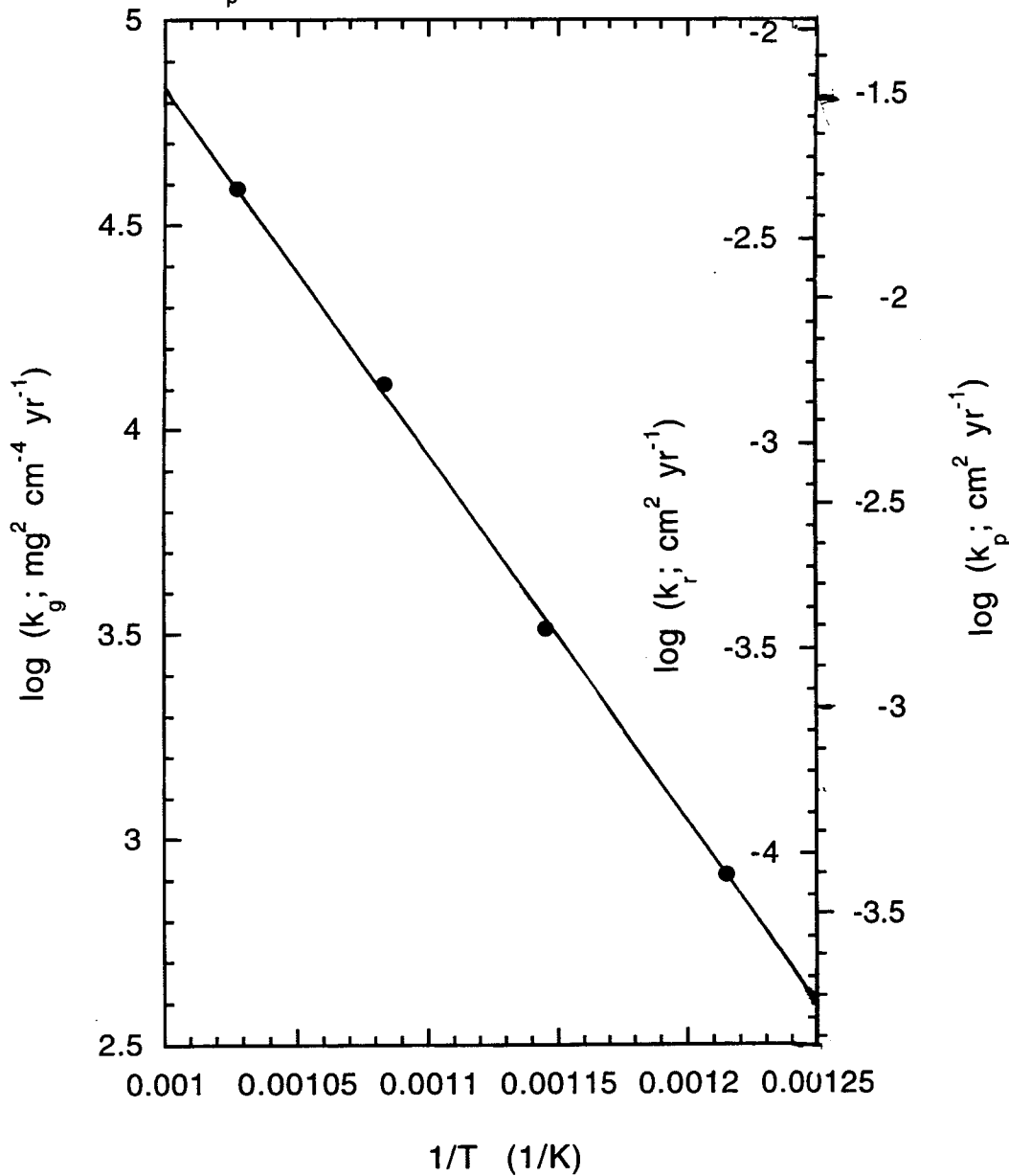


Figure 4-3. Temperature-dependence of the parabolic rate constants during the oxidation of Fe-2.25Cr-1Mo in dry oxygen [Simms and Little (1987), reprinted by permission from Plenum Publishing Corporation]

weight gain equals 12 mg/cm², as suggested from the results of Simms and Little (see Figure 4-4). Of course, breakaway oxidation for iron does not mean that the residual metal is rapidly consumed to completion; rather, in the worst case, a repeat of the initial parabolic kinetics should be expected.

From the parabolic rate constants listed in Table 4-2, the mass gain, thickness of the oxide scale, and recession thickness for a period of 1,000 years of oxidation were calculated, using Eqs. (4-7c) and (4-8b). The results are given in Table 4-3.

A Cr- (and Mo-) enriched spinel layer close to the metal was also observed in another study (Christl et al., 1989) during oxidation in air at 600 °C. The inner magnetite-rich spinel phase adhered to the metal substrate while the outer part of the scale, consisting mainly of hematite, spalled upon cooling. Compressive stresses were generated only in the hematite layer, the magnetite layer being in tension. During cyclic oxidation between 400 and 550 °C, a one-layer magnetite scale was formed. For the Yucca Mountain repository project, the cooling of the containers will be so slow and the temperature variation so small (e.g., from 300 °C to 100 °C in 1,000 years) that breakaway due to the difference in thermal expansion coefficients (such as is observed during thermal cycling) will not occur.

Table 4-3. Mass gain ($\Delta m/A$), thickness of the oxide scale (X), and recession thickness (R) calculated for a period of 1,000 years of oxidation in dry oxygen

Temperature (°C)	$\Delta m/A$ (mg/cm ²)	X (mm)	R (mm)
300	3.66	25.2	12.0
275	1.60	11.0	5.2
250	0.65	4.5	2.1
225	0.239	1.6	0.78
200	0.080	0.55	0.26
175	0.0234	0.16	0.077
150	0.0059	0.041	0.019
125	0.00127	0.0088	0.0042
100	0.00022	0.0015	0.0007

Raman et al. (1992) showed that the oxidation rate of Fe-2.25Cr-1Mo in air at 550 °C decreased with increasing alloy grain size. Micrographs clearly showed preferential oxidation along alloy grain boundaries that caused some grains to detach from the alloy substrate. The oxides were solid solution spinels containing various levels of Fe, Cr, and Mo. The standard Gibbs energy of formation of FeCr₂O₄ is greater than that for Fe₃O₄ (Bittner et al., 1980). The formation of Cr-rich oxides is therefore favored. Oxides formed at the alloy grain boundaries are found to be much richer in Cr than those formed over the grains. The oxidation front progressed along the boundaries first and then toward the center of an oxidizing alloy grain. Finally the entire grain was consumed as an oxide. Because of the formation of Cr-rich oxides essentially at the grain boundaries, the outward diffusion of Cr to the scale is suppressed. For any grain size investigated (from 16 μm to 59 μm), the Cr content throughout the inner scale was not sufficient to form a protective layer of Cr-rich oxide. Small-grain-size alloy specimens oxidized faster than large-grain-size specimens, producing thicker scales, leading to more cracking and spalling at 550 °C (Raman et al., 1992). However, in all cases, parabolic kinetics were observed. The weight gain of an alloy specimen with 16 μm grain size during 6 hours oxidation at 550 °C was double the weight gain of a specimen with 59 μm grain size, oxidized for the same duration. The oxidation rate was found to be roughly inversely proportional to the grain diameter.

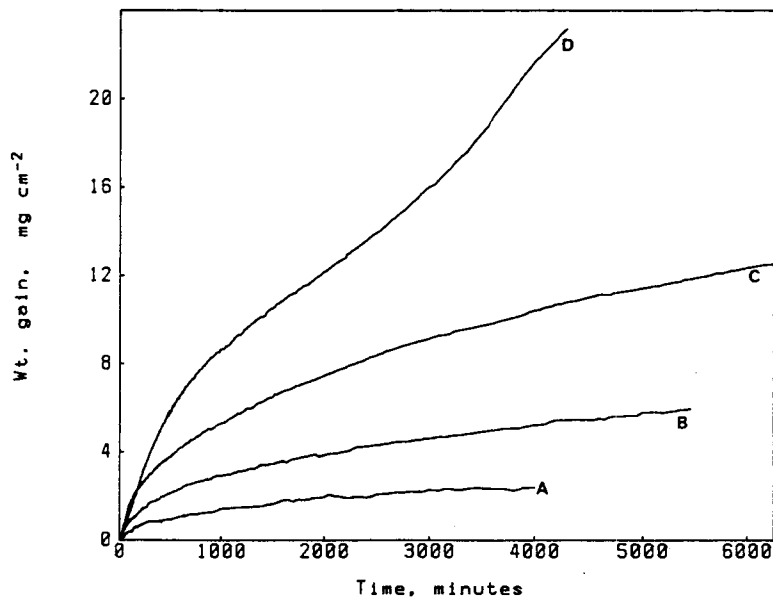


Figure 4-4. Oxidation of Fe-2.25Cr-1Mo in dry-flowing oxygen for periods up to 100 hours. (A) 550 °C. (B) 600 °C. (C) 650 °C. (D) 700 °C. Curve (D) indicates that breakaway occurs for a weight gain of about 12 mg/cm². [from Simms and Little (1987), reprinted by permission from Plenum Publishing Corporation]

This grain size dependence is in contrast with that reported for Cr-rich alloys, such as Ni-Cr, stainless steels and Alloy 800 (Giggins and Pettit, 1969; Leistikow et al., 1987; Shida et al., 1983; Kokowa and Nagata, 1981). For such Cr-rich ($N_{Cr} \geq 0.20$) alloys, a decrease in the grain size increases the diffusion paths (grain boundaries) in the alloy near the surface, resulting in enhanced selective Cr oxidation and hence in more rapid formation of a complete layer of protective Cr_2O_3 . As a result, for these high-Cr alloys, the formation of a complete Cr-rich protective layer takes place because the preferential formation of Cr_2O_3 occurs at and around the alloy grain boundaries. On the other hand, in the case of a "dilute" alloy with much lower Cr content, such as Fe-2.25Cr-1Mo steel, irrespective of its grain size, outward grain boundary diffusion of Cr is never sufficient to allow the lateral growth of Cr_2O_3 to form a continuous protective oxide layer at the external surface. At temperatures of 400–550 °C, the scale growth rate (including lateral growth) is sufficiently low that the number of oxide nuclei depend on the surface defect density [e.g., interphase (carbide/ferrite) and grain boundaries]. Therefore, for this temperature range, the size of the oxide grains depends on the size of the alloy grains. For a much lower temperature range (100–300 °C), the grain size or carbide dispersion should not be important as the expected oxide grain size would be much smaller than these features.

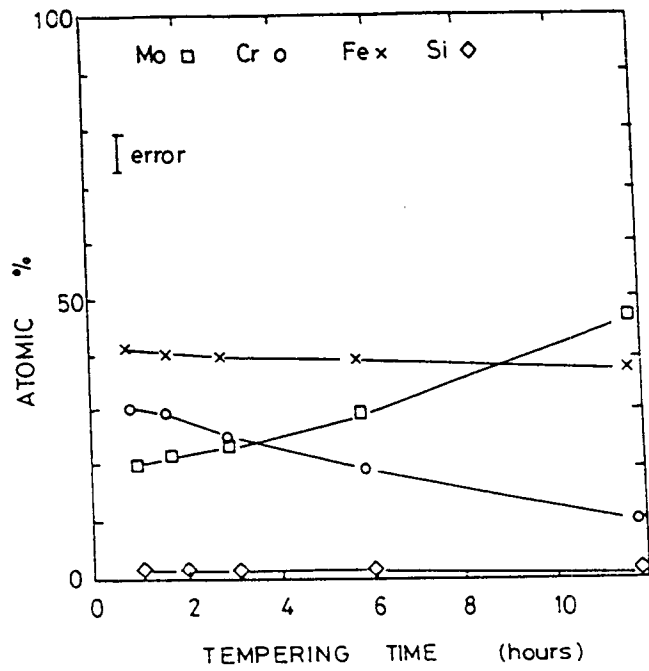
The composition of the inner oxide layer of a related ferritic alloy, Fe-2.25Cr-1MoNb, oxidized at 501 °C was investigated by Hurdus et al. (1990). As in the case of Fe-2.25Cr-1Mo, the diffusion in the scale of Fe-2.25Cr-1MoNb takes place almost entirely by outward diffusion of Fe^{3+} along the scale grain boundaries. Fine-grain (0.04 μm) oxide layers of Fe-2.25Cr-1MoNb were found to contain levels of Cr, Mo, and Si that were on average three times higher than in the coarse-grain (0.2 μm) layers. Higher local levels of Cr and Si in the magnetite scale should contribute to a more protective layer.

The alloy grain size depends on the type of heat treatment experienced by the alloy during its processing. The oxidation behavior of Fe-2.25Cr-1Mo has indeed been found to vary according to the annealing, normalizing, quenching, and tempering procedures (Khanna et al., 1987). Tempering, for example, promotes the extent of the transformation of Fe_3C into Mo- and Cr-containing carbides (Pilling and Ridley, 1982). Carbides of stoichiometries M_7C_3 , M_{23}C_6 , M_2C , and M_6C were detected in Fe-2.25Cr-1Mo tempered at 700 °C. The compositions of M_{23}C_6 and M_7C_3 were $\text{Cr}_{8.4}\text{Fe}_{12.0}\text{Mo}_{2.6}\text{C}_6$ and $\text{Cr}_{4.2}\text{Fe}_{2.4}\text{Mo}_{0.4}\text{C}_3$. The compositions of M_6C and M_2C as a function of tempering time are given in Figures 4-5 and 4-6. From these figures, an increase in tempering time for Fe-2.25Cr-1Mo results in an increase of the molybdenum contents of M_6C and M_2C , and a decrease of their iron, chromium, and silicon contents. The equilibrium structure depends on the (Cr+Mo):C ratio, which means that a decrease in the carbon content of the alloy has the same effect on carbide composition as increasing the Cr+Mo content while maintaining the carbon level constant. An increase in the Mo:C ratio promotes the formation of a greater volume fraction of M_6C , although it was still limited to 1 percent after 3 hours of tempering. A reduction in the carbon content from 0.09 to 0.06 percent displaced the equilibrium from M_3C_6 , and M_2C in ferrite to one of M_6C , M_{23}C_6 and M_7C_3 in ferrite. The rate at which the carbide replacement reactions take place increases as the carbon content in the steels is reduced. Most of the cementite (Fe_3C) reacts totally to form Mo- and Cr-containing carbides within 30 minutes of tempering at 725 °C (Khanna et al., 1987). The decrease in the Cr content of the alloy due to these reactions probably leads to a lowering of its oxidation resistance, because less Cr is available for outward diffusion.

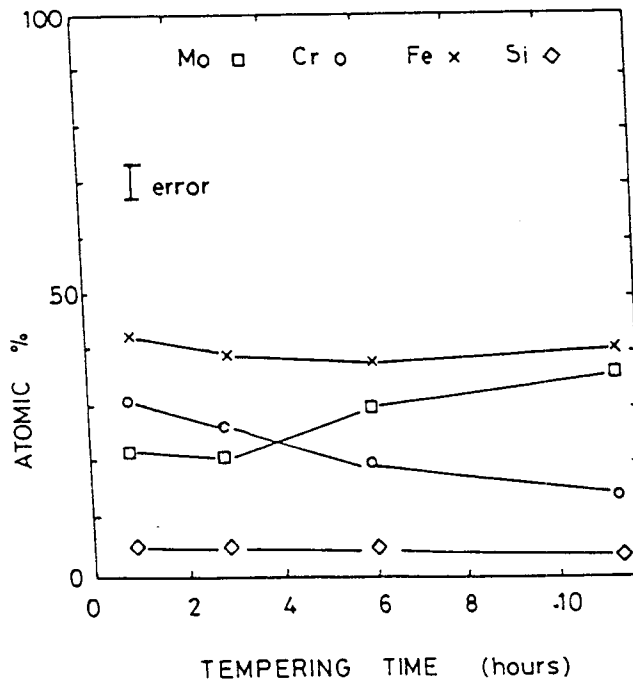
The effect of tempering time at 725 °C on the oxidation behavior of Fe-2.25Cr-1Mo in air has been studied further (Raman et al., 1988). The ferrite grains coarsened as the tempering time increased from 10 to 180 minutes. Tempered samples were oxidized for 1,000 hours at 500 °C. Needle-shaped oxide particles were observed on the entire surface of the samples. The oxidation behavior, without considering the spalled scale, approximately followed parabolic kinetics. By contrast, linear oxidation behavior was recorded when the weight of the spalled layer was included. The oxidation rate initially decreased as the tempering time increased from 10 to 60 minutes, but then increased with further increase in tempering up to 180 minutes. All the specimens started spalling after about 500 hours of isothermal oxidation at 500 °C. Such breakaway oxidation typically occurs at a certain thickness of the oxide layer, when compressive stresses reach a critical value. These stresses lead to *in situ* cracking and spalling of the oxide layer, as a result of which, faster molecular ingress of oxygen occurs, leading to a temporarily higher oxidation rate. This breakaway period of 500 hours observed during oxidation in air at 500 °C is much shorter than the value calculated for the same temperature (4,300 hours) from the data of Simms and Little obtained in oxygen. However, this difference in high-temperature breakaway periods is not critical in view of the much longer low-temperature breakaway periods (and the corresponding low-temperature slow oxidation kinetics).

An acoustic emission (AE) study of the spalling of oxidized Fe-2.25Cr-1Mo allowed the identification of three basic processes, namely pre-breakaway, post-breakaway, and internal cracking (Jha et al., 1986). The pre-breakaway region has a wide AE spectrum indicating that many processes like dislocation climb, grain-boundary sliding, etc. are involved during plastic deformation of the scale. The post-breakaway is characterized by a higher frequency peak which is linked to crack nucleation. During cooling, a low-frequency AE signal is recorded, which is related to spalling/internal cracking of the oxide layer (i.e., to a cleavage type of crack propagation).

The AE signals of samples that were oxidized in air in the range 600–950 °C and cooled down to room temperature were recorded (Figure 4-7) (Khanna et al., 1985). These AE signals, as well as micrographs of the scales obtained after the test clearly show that the extent of spalling increases with increasing temperature drop. From these results, an alloy oxidized at a temperature below 600 °C and cooled to



(a)



(b)

Figure 4-5. Variation in composition of M_6C on tempering at 700 °C; (a) steel with 0.18% C, (b) steel with 0.06% C [Pilling and Ridley (1982), reprinted with permission from The Minerals, Metals & Materials Society]

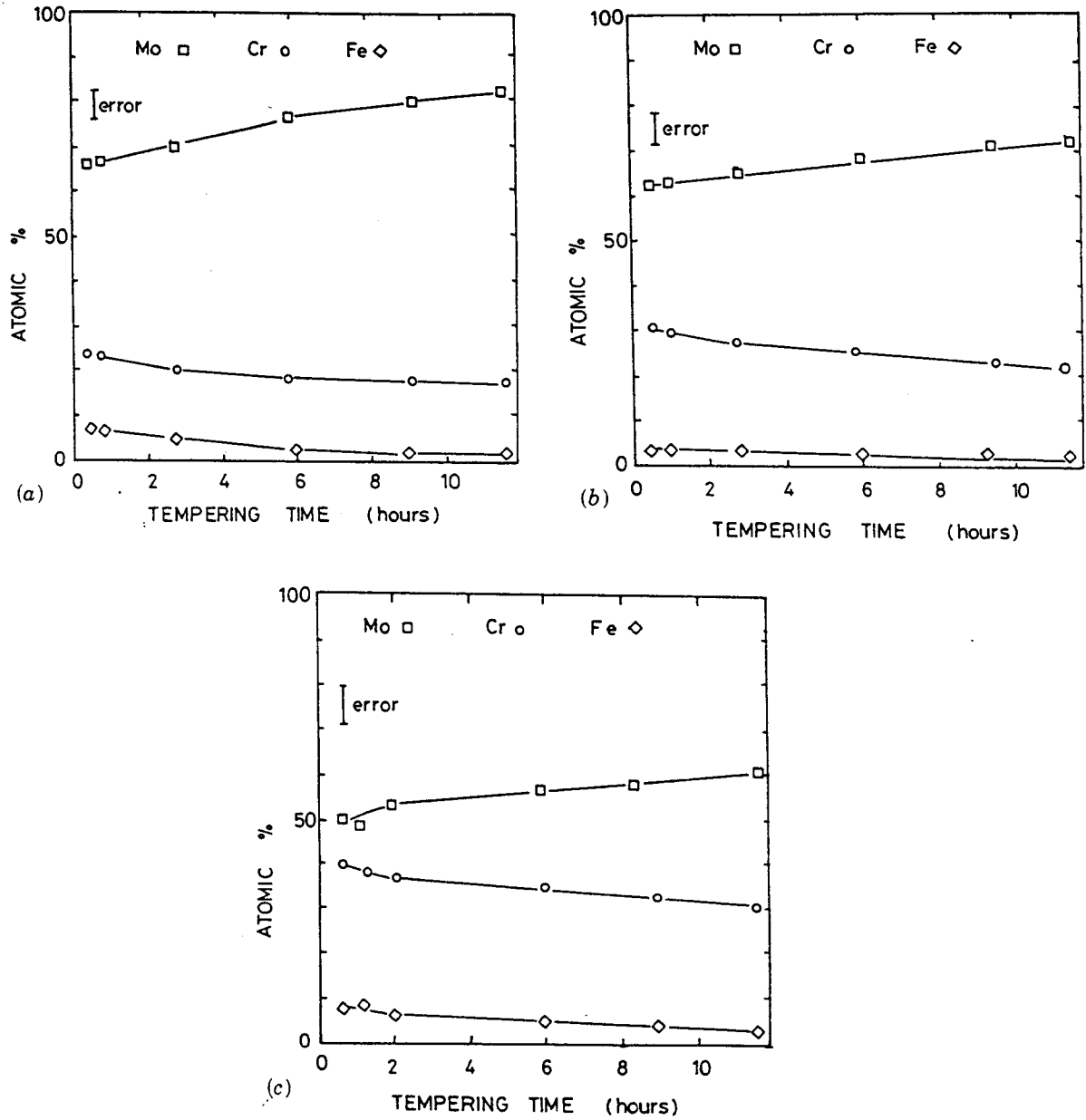


Figure 4-6. Variation in composition of M_2C on tempering at 700 °C; (a) steel with 0.18% C, (b) steel with 0.06% C, (c) steel with 0.09% C [Pilling and Ridley (1982), reprinted with permission from The Minerals, Metals & Materials Society]

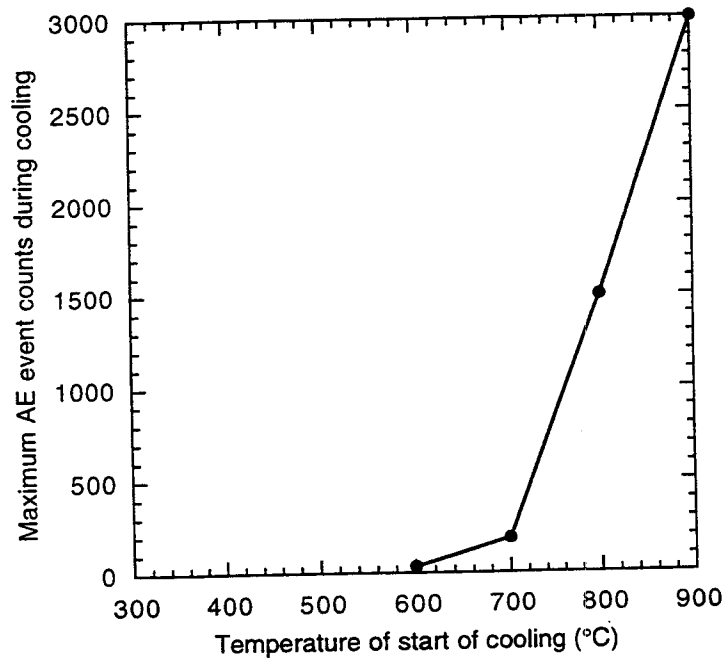


Figure 4-7. Acoustic emission (AE) signals of samples that were oxidized in air at temperatures in the range from 600–950 °C and cooled down to room temperature. These AE signals as well as micrographs of the scales obtained after the test clearly show that the extent of spalling increases in temperature from which the cooling starts. [Khanna et al. (1985), reprinted with permission from Plenum Publishing Corporation]

room temperature will have very little tendency to spall. For the Yucca Mountain repository project, the initial temperature of 300 °C means that no cooling-induced spalling is expected to occur.

As a summary, lower oxidation rates are obtained with steels having large grain size (60 μm or more, to suppress grain boundary oxidation). Low carbon content an optimum tempering schedule would minimize the Cr trapped in the form of Cr carbides, and should lead to a lower oxidation rate with less preferential grain boundary oxidation.

5 POSSIBILITY TO REDUCE THE SCALING RATE

5.1 REACTIVE ELEMENT EFFECT

For more than 50 years, the high-temperature corrosion community, and especially the companies which manufacture and market alloys for high-temperature service, have been acutely aware of a very favorable phenomenon called the Reactive Element Effect (REE). Some detailed discussion of the REE is presented here, because it is thought that a simple and inexpensive treatment of steel containers could be achieved to take advantage of this beneficial effect, as discussed later. According to the REE, a small content of certain very reactive elements (about 0.02 percent or the like, depending on the alloy and the choice of RE) cause a very great improvement in the scaling behavior of alloys which form chromia or alumina scales (e.g., Fe-Cr, Ni-Cr, Co-Cr, NiAl and related commercial alloys). In particular, four effects are well documented for Cr_2O_3 -forming alloys: (i) the scales exhibit much better adherence, especially for oxidation with rapid temperature cycling; (ii) an alloy is able to form an exclusive Cr_2O_3 scale for alloy compositions containing low-Cr contents; (iii) the parabolic scaling rate constant can be greatly reduced, by as much as a factor of 100, with a greater reduction for lower temperatures; and (iv) the scaling mechanism changes from outward cation diffusion (using cation interstitial and vacancy defects, preferentially at grain boundaries) to inward oxygen anion diffusion, also at grain boundaries.

Figures 5-1 (Patibandla et al., 1991), 5-2 (Przybylski et al., 1988), and 5-3 (Hussey et al., 1989) illustrate the reduction in scaling kinetics at high temperatures for Ni-Cr, Co-Cr and Fe-Cr alloys where different REs have been introduced in different ways. Similar kinetics plots for cyclic oxidation would show an even more striking favorable effect.

For such alloys, and also for Al_2O_3 -forming alloys, small contents of elements such as yttrium, cerium, lanthanum, zirconium, etc., which form very stable oxides and have a very large cation size compared to the host Cr^{3+} or Al^{3+} , can be introduced into the alloy or at its surface in a number of effective ways: (i) as an alloy addition, which usually forms an intermetallic compound particle in the grain boundaries of the alloy; (ii) in the form of a dispersed oxide phase [e.g., as in oxide dispersion strengthened (ODS) alloys]; (iii) by ion implantation into the surface layer, (iv) by the deposition onto the surface of some powder or gel or some evaporated or sputtered deposit; or (v) as the product of a surface anodic polarization in an aqueous solution containing the desired RE solute (Whittle and Stringer, 1980; Stringer, 1989; Moon, 1989; Pieraggi and Rapp, 1993). The different methods offer a difference in reliability to achieve the REE, with the alloy addition normally preferred, if this can be achieved practically. In fact, cerium deposition from aqueous solutions has also been observed to effect a reduction in the aqueous corrosion rate for alloys forming alumina or chromia passive films, and the appropriate mechanism may be common with the high temperature mechanism. Today, the aqueous corrosion community empirically credits the rate reduction to retardation in the cathodic reduction reaction in response to a sort of surface coverage by the strongly adsorbed, highly charged cation (Mansfeld et al., 1990; Davenport et al., 1991; Aldykewicz et al., 1995).

5.2 MECHANISMS FOR THE REACTIVE ELEMENT EFFECT

The mechanism for the high-temperature REE continues to be controversial, but there are now three "favored" mechanisms. The "Sulfur Effect" was introduced by Funkenbusch et al. (1985), Smeggil et al. (1986), and supported by Smialek (1991) to rationalize the effectiveness of yttrium in reducing scale spallation in the growth of alumina scales on superalloys and NiAl-base coatings. This suggested

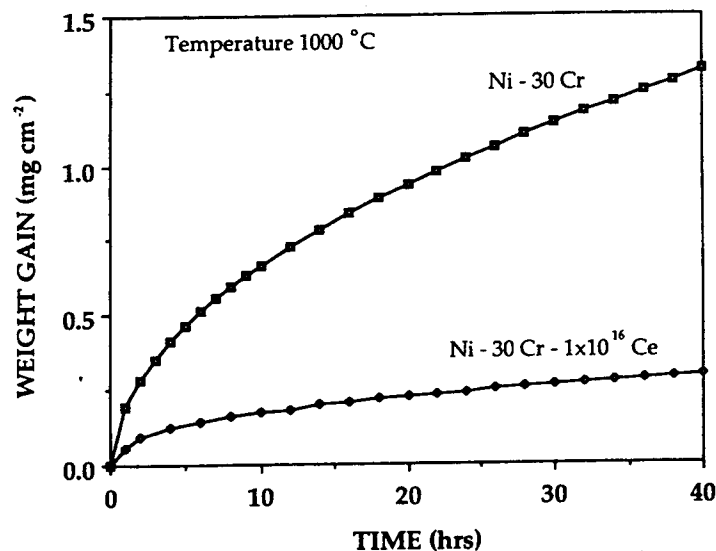


Figure 5-1. Oxidation kinetics of unimplanted and implanted (with 10^{16} ion/cm² Ce) Ni-30 Cr alloys at 1,000 °C in a 80 mole percent (m/o) CO:20 m/o CO₂ gas mixture [Patibandla et al. (1991), reprinted with permission from The Electrochemical Society, Inc.]

mechanism notes that yttrium (and other REs) form very stable sulfides, and when used as an alloying addition, the RE will tie up sulfur upon solidification as a sulfide or oxysulfide particle to greatly reduce sulfur as a solute in the solid solution. Sulfur is known to segregate strongly to the grain boundaries and free surfaces of alloys at high temperatures, and the proposed Sulfur Effect mechanism supposes that sulfur also strongly adsorbs at even a totally adherent metal/scale interface, where it weakens the chemical bond between the metal and the scale, so that scale spallation occurs upon temperature cycling. Clearly, the trapping of solid solution sulfur is indeed advantageous, and today the superalloy and coating communities are striving (with success) to greatly reduce the total sulfur content of alloys and coatings (to a few ppm S) so that the deleterious amount of sulfur is eliminated. Then the RE addition, which is difficult to introduce anyway (e.g., during the solidification of superalloy single crystals), would not be needed. However, while realization of the Sulfur Effect has been useful and important practically, the originally proposed mechanism is not correct in detail. By careful Auger spectroscopy analyses through alumina scales, Grabke et al. (1991) have shown that sulfur is not adsorbed at a site of total (semi-coherent, epitaxial) metal/scale adherence, but only at interfacial sites where metal/scale separation has already occurred. Such interfacially adsorbed sulfur should stabilize a decoherence of the scale from the metal by reducing the surface tension of the alloy/gas (void) interface, but not cause it because of “bond weakening.” Furthermore, the Sulfur Effect does not explain the advantageous effects of the RE when sulfur is not involved anyway.

The second tentative REE mechanism is called the “Grain Boundary Segregation” mechanism, which was originally proposed by Przybylski et al. (1988) and Cotell et al. (1990), and supported more recently by Pint (1996). Because the REs have very large ion sizes, generally about 45 percent greater than the host Al³⁺ or Cr³⁺ cations of alumina or chromia scales, the RE cations are only very slightly soluble in the oxide lattices and are, therefore, found to be segregated at both the metal/scale interface and at the grain boundaries of the scale. In the absence of any RE, the growth of chromia is limited by the outward diffusion of Cr³⁺ cations both by interstitials and over vacancies at the grain boundaries of

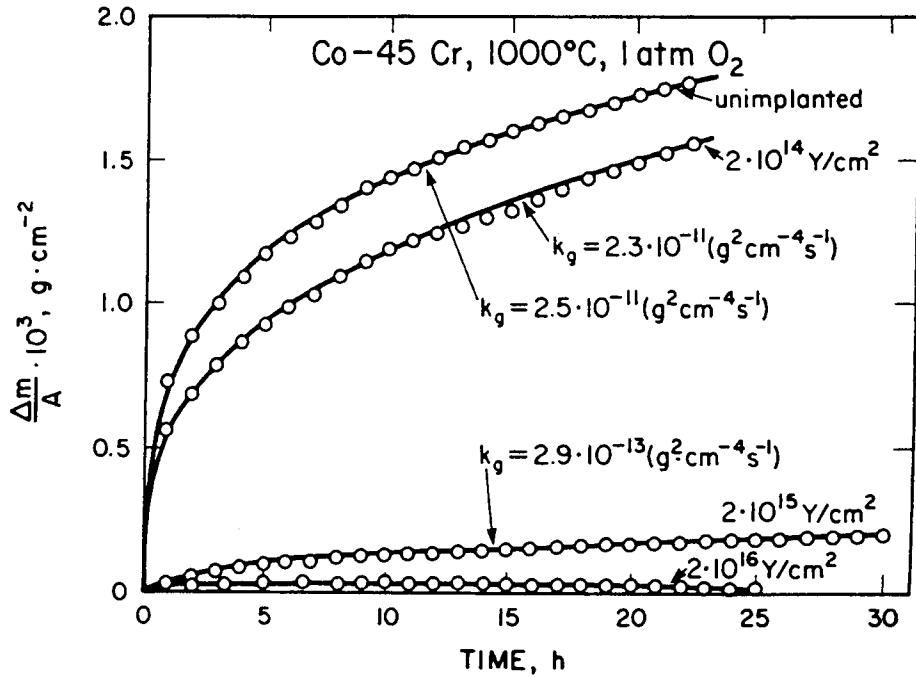


Figure 5-2. Weight gain per unit area as a function of time showing the influence of the dose of implanted yttrium on the rate of oxidation of a Co-45Cr alloy at 1,000 °C in pure oxygen [Przybylski et al. (1988), reprinted with permission from The Electrochemical Society, Inc.]

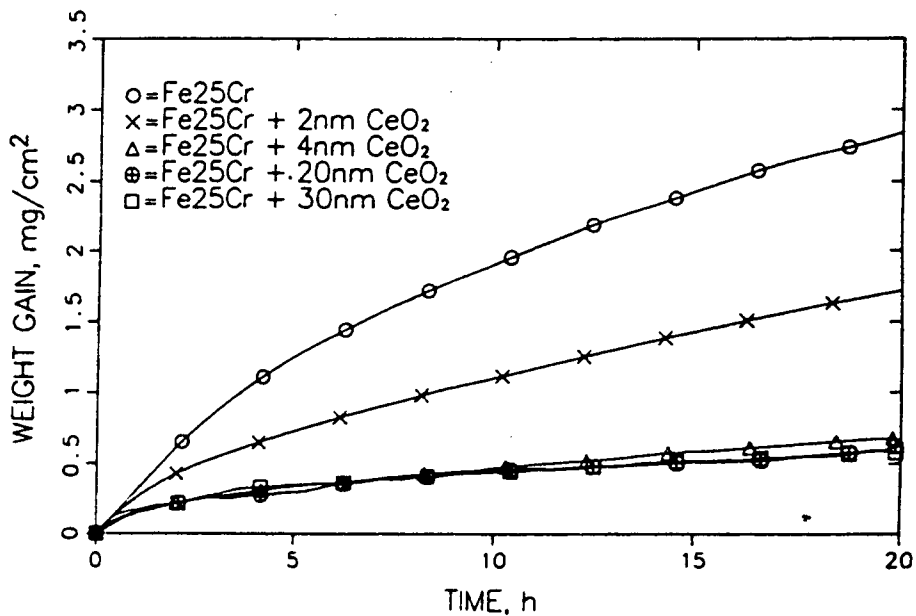


Figure 5-3. Oxidation kinetics at 1100 °C of a Fe-25Cr base alloy and a base alloy coated with 2, 4, 20, and 30 nm CeO₂. 1 mg/cm² ≈ 6.1 μm of oxide. [Hussey et al. (1989), reprinted with permission from Elsevier Science S.A.]

the scale. Because the REs are known to segregate at the scale grain boundaries, the Grain Boundary Segregation mechanism supposes (without any direct evidence) that the RE ions block the outward diffusion of cations but permit the slower inward diffusion of oxygen anions. A similar explanation is used for the REE in alumina scale growth, except that alumina scales often begin growth in the γ or δ crystalline modifications which grow by outward cation diffusion, while the steady-state α (corundum) scale grows by grain boundary oxygen ion diffusion anyway. Pint (1996) has observed that at very high temperatures, the RE migrates outward over the scale grain boundaries and is then concentrated at the external surface. For this reason, the addition of REs by ion implantation may be inadequate for a continuing REE, as the amount of available RE is limited and ultimately lost to the external surface (for very high temperatures). In criticism of the Grain Boundary Segregation mechanism (i.e., that the RE segregation to the scale grain boundaries changes the dominant diffusion mechanism for the scale), one can mention that RE segregation at oxide scale boundaries is not always observed, and in fact, there have been no direct measurements to support the hypothesis that grain boundary diffusivities are really changed in the manner proposed. Even when segregation of RE at the scale grain boundaries is observed, this does not necessarily identify this segregation as the dominant factor in the REE.

The third, most recent, REE mechanism, the "Poisoned Interface Model" was proposed by Pieraggi and Rapp (1993) and supported by Strawbridge and Rapp (Strawbridge and Rapp, 1994; Strawbridge et al., 1995). As explained by Hirth, Pieraggi, and Rapp (Hirth et al., 1995; Pieraggi et al., 1995), the metal/scale interface must serve as the site to create or annihilate point defects which support the diffusion mechanism for scale growth. Usually at high temperatures, diffusion through the scale, and not the interfacial reaction, is the rate limiting step, providing global parabolic scaling kinetics. The creation or annihilation of point defects (vacancies or interstitials) at the metal/scale interface is achieved by the climb of interfacial dislocations, both misfit and misorientation dislocations. For a cation-diffusing scale, the blockage of the relevant interfacial step for defect creation or annihilation would prohibit scale growth by the outward cation diffusion mechanism, leading to an alternative growth mechanism (e.g., inward oxygen ion diffusion). Because of their large ionic size, RE ions are known to segregate to the metal/scale interface, and this model supposes that the segregated REs elastically pin the interface dislocations supportive of cation diffusion and inhibit their climb. Figure 5-4 (Strawbridge and Rapp, 1994) provides a schematic drawing for the Poisoned Interface Model. Because the climb of interfacial dislocations is blocked, cation diffusion is replaced by slower inward anion diffusion. This scenario is consistent with the facts about the REE, and only a very small fraction of a monolayer of segregated REs at the metal/scale interface is thought to be sufficient to block cation diffusion. However, high resolution hot-stage transmission electron microscopy (TEM) observations to support this proposed mechanism have not yet been achieved, and indeed will be difficult.

5.3 APPLICATION OF REACTIVE ELEMENT EFFECT TO STEEL CONTAINERS

The transference of the REE observed dominantly for the growth of chromia and alumina scales to other scales, even those oxides grown on the pure metals Fe, Ni, Co and Cu, was demonstrated by Strawbridge and Rapp (1994). According to the Poisoned Interface Model, the blocking of the interfacial reaction step for a cation-diffusing scale by dislocation pinning using a proper RE segregant should enjoy quite general application, if one only chooses the proper segregant. Strawbridge and Rapp (1994) proposed (as a first approximation) that a favorable ionic size ratio of the RE to the host cation could serve as a basis for choosing the particular RE segregant for a given metal/scale interface. For the growth of chromia on alloys, the most effective REs yttrium and cerium each have an ionic size that is about 45 percent greater than that for Cr^{3+} , so an ionic size ratio $r_{\text{RE}}/r_{\text{host}}$ equal to 1.45 was predicted to provide

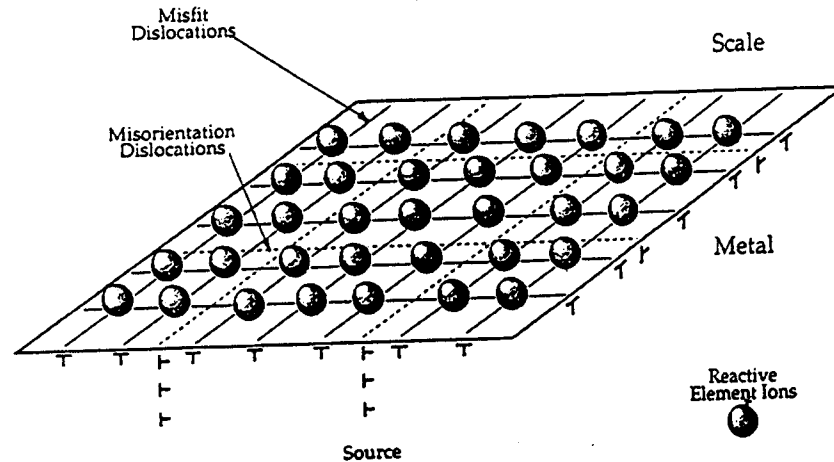


Figure 5-4. Schematic representation of the “poisoned-interface” interpretation of the reactive element effect. Large, highly charged reactive element ions segregate to metal/scale interface, thereby pinning the misfit dislocations and preventing scale growth by cation diffusion. [Strawbridge and Rapp (1994), reprinted with permission from The Electrochemical Society, Inc.]

the necessary interfacial segregation for the REE for any metal/scale system. This hypothesis was tested by evaporating only 250 Å of the alkaline earth metals Ca, Ba and Sr onto the polished surfaces of each of the pure metals Fe, Ni, Co and Cu. For the oxidation in air for each of these four pure metals, that alkaline earth deposit with an ionic radius ratio closest to 1.45 gave the greatest reduction in the parabolic rate constants. This result is illustrated in Figure 5-5 from Strawbridge and Rapp (1994). In fact, the oxidation conditions were not chosen to maximize the magnitude of the REE, because the chosen oxidation temperatures were too high. Nevertheless, a maximum rate reduction was observed for each of the four metals for the specific RE with the optimum ionic radius ratio. For pure iron, strontium proved to be the optimum RE, but scaling was only studied at 600 °C. A much greater effect (greater rate reduction) would be expected at a lower scaling temperature.

For the scaling of pure nickel at 1,000 °C, the parabolic rate constant was reduced by a factor of 4.4 by 250 Å of Ca. But for the scaling of Ni at 850 °C, the rate constant was reproducibly reduced by a factor of 20, as shown in Figure 5-6, and the scale growth mechanism was clearly changed from the usual outward cation diffusion to inward anion diffusion. Gonzales et al. (1996) supported this observed rate reduction for the scaling of pure nickel by the preliminary deposition of a Ca-rich anodic oxidation film from an $\text{Ca}(\text{NO}_3)_2$ -doped aqueous solution. Upon oxidation at 600 °C, the parabolic rate constant for the oxidation of pure nickel was reduced by a factor of 100. Upon extrapolation, for a further reduction in the oxidation temperature, an even greater reduction in the rate constant could be expected.

There is then reason to expect that the preliminary introduction of the proper RE at the external surface of a steel prior to oxidation at a low temperature could effect a very great reduction in its oxidation rate, and perhaps also its rate of aqueous corrosion. At this time, strontium or calcium would seem to be the favored RE for doping the Fe/Fe₃O₄ interface of steels. But some simple experimentation with these and other REs with similar ionic sizes could establish the optimum segregant. The method introduced by Gonzales et al. (1996) (i.e., deposition of the RE into an anodic oxide from an aqueous

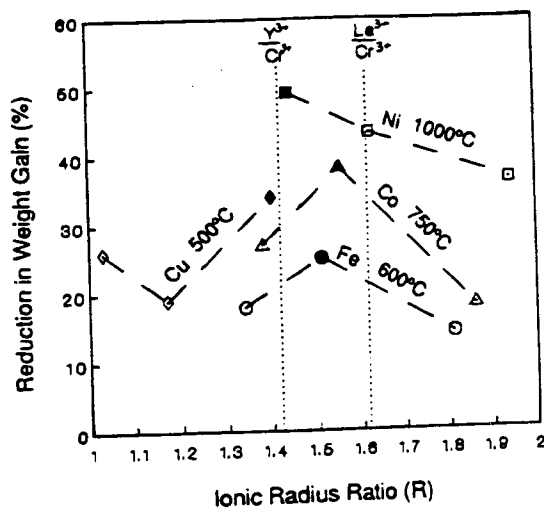


Figure 5-5. Trends in reduction of weight gain (compared with uncoated samples) after oxidation in 1 atm O₂ for 24 h for pure metals with evaporated coatings of 250 Å Ba, Ca, or Sr. Oxidation at 1,000 °C for Ni, 750 °C for Fe, and 500 °C for Cu. Ionic radius ratio, $R = r_{RE}/r_{metal}$. [Strawbridge and Rapp (1994), reprinted with permission from The Electrochemical Society, Inc.]

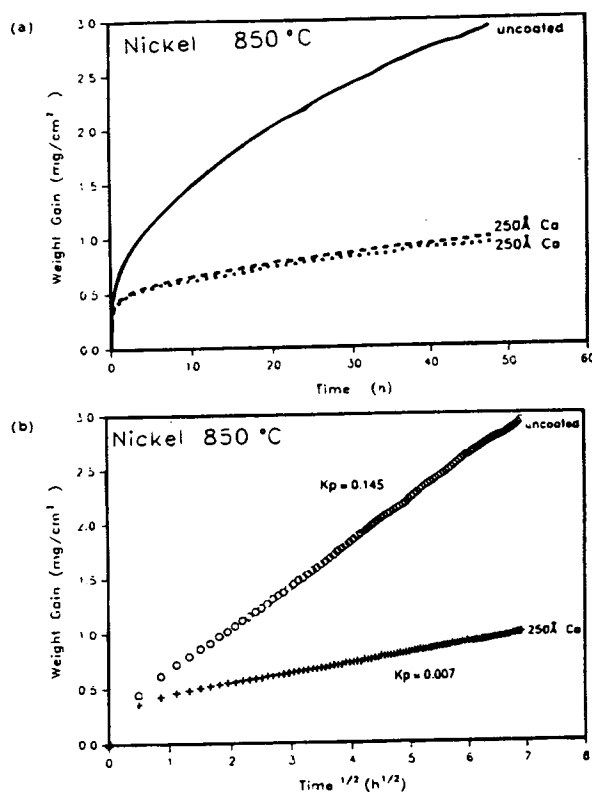


Figure 5-6. Oxidation kinetics for pure Ni coupons with and without 250 Å films of Ca, in 1 atm O₂ at 850 °C: (a) Weight gain with time; (b) Pieraggi plot [Strawbridge and Rapp (1994), reprinted with permission from The Electrochemical Society, Inc.]

solution) would seem to be the easiest, cheapest, and most reliable means to introduce the interfacial segregant. The oxidation testing needed to demonstrate the expected reduction in the oxidation rate would probably be conducted at temperatures around 500 °C, far above that projected for the repository. Otherwise, the scaling kinetics would probably be so low that no existing kinetics apparatus (e.g., thermogravimetric analyses) could make the measurements in a reasonable time. Such experimentation is recommended prior to the fabrication of the steel containers.

6 SUMMARY, CONCLUSIONS, AND RECOMMENDATIONS

For the HLW repository site at Yucca Mountain, Nevada, the outer surface of the buried waste containers is expected to be exposed to dry atmospheres for thousands of years at temperatures slowly decreasing from 300 °C. During the first 1,000 years, the initial radioactivity of the HLW is supposed to decrease by over 99 percent leading to container temperatures of about 100 °C. For this reason, the expected oxidation behavior of the candidate materials for the outer overpack of the containers, carbon steels and Fe-2.25Cr-1Mo steels, was estimated for a period of 1,000 years for temperatures in the range 100–300 °C. The extrapolation of the existing data according to a parabolic kinetics law with an Arrhenius temperature dependence assumes that a dense uniform scale is formed and that the scale growth kinetics are limited by solid-state (grain boundary) diffusion through the dense scale. Where data were available, predictions of times for scale rupture resulting in breakaway oxidation were also made, but this phenomenon is not significant at such low temperatures. In dry atmospheres in this low-temperature range, the candidate materials form scales consisting of only two oxide phases: Fe₃O₄ (magnetite) at the surface of the alloy, and Fe₂O₃ (hematite) between the magnetite layer and the gas phase. For an oxidized low-alloy steel, the thickness of the magnetite layer is approximately six times the thickness of the hematite layer. After a relatively short transient period with a logarithmic time-dependence, the oxidation kinetics follow a parabolic rate law, which was used to make extrapolations.

The scaling rates of low-carbon steels at low temperatures increase with increase in carbon content, and with increase in the fineness of the Fe₃C dispersion in ferrite. Runk and Kim (1970) provided excellent and relevant studies of Fe-C oxidation at 200–350 °C which were used for extrapolation to very long times. During a period of 1,000 years at 250 °C, for abraded carbon steels having a fine pearlitic microstructure and containing 0.2 wt% C, dry oxidation is expected to consume only 4.1 μm of the alloy surface. Even less metal recession is expected for carbon steels with spheroidized C and a chemically etched surface. While most of the studies in the literature used surfaces prepared by abrasion, chemically polished or etched surfaces oxidize much more slowly at low temperatures, although the adherence of the scale to the metal is locally broken (Caplan and Cohen, 1966). From the calculations presented in this report, the ratio of the metal recession depth formed during 1,000 years of oxidation on a carbon steel with a spheroidized carbide phase to that formed on a fine pearlitic carbon steel is 0.56. This means that 2.3 μm of abraded Fe-0.2 wt% C steel is predicted to react at 250 °C, but even this depth could be lowered by chemical surface preparation. Decarburization of carbon steels upon oxidation at such low temperatures of the HLW canisters is not expected to occur.

In the case of Fe-2.25Cr-1Mo steels, the oxidation studies found in the literature were conducted only at 500 °C and higher. So the extrapolation of the data of Simms and Little (1987) to much lower temperatures and for very long times is somewhat precarious. For 1,000 years of dry oxidation at 250 °C, abraded Fe-2.25Cr-1Mo steels are expected to recede only 2.1 μm. Cold work of the surfaces by abrasion increases the number of dislocations, which leads to a higher vacancy annihilation capability and less tendency for vacancies to accumulate and form voids or discontinuities at the metal/scale interface. Consequently, cold work leads to a better contact between the steel and the oxide scale, but also a higher oxidation rate. In fact, for such very thin oxide films, cracking and spallation are not expected to occur.

Low-temperature oxidation proceeds mainly by grain boundary diffusion in the magnetite scale, so that a small grain size in the scale leads to a higher oxidation rate. Raman et al. (1992) showed that the oxidation rate of Fe-2.25Cr-1Mo in air at 550 °C decreased with increasing alloy grain size. At 550 °C, oxidation progresses preferentially down along substrate grain boundaries and causes some grains to

detach from the alloy substrate. Finally, the outermost alloy grains are completely consumed as oxides. Tempering of Fe-2.25Cr-1Mo affects the oxidation behavior in two ways. First, a resulting coarsening of the grains decreases the oxidation rate. Second, the formation of Cr-rich carbides increases the oxidation rate. The lowest oxidation rate was realized for tempering at 725 °C for 60 minutes.

The data analyzed in this report indicate that carbon steels and low alloy steels have very similar oxidation kinetics at low temperature for extended periods of time. Therefore, either Fe-0.2 wt% C steel with spheroidized carbide, or low-carbon, large grain (60 μm or more) Fe-2.25Cr-1Mo steel with optimum heat treatment are good choices of materials for the outer containment barrier of the HLW containers. Chemical etching/polishing would serve to minimize the oxidation kinetics.

A further preliminary surface treatment, optimized to instigate the REE is also discussed and recommended to further improve the oxidation resistance. From the current knowledge of the REE, the introduction of the proper RE at the external surface of a steel prior to oxidation at a low temperature could effect a very great reduction in its oxidation rate, and perhaps also its attack by aqueous corrosion. At this time, strontium or calcium would seem to be the favored RE for doping the Fe/Fe₃O₄ interface of steels. However, some preliminary research would be required to establish the optimum segregant and develop the necessary surface processing procedures.

7 REFERENCES

- Aldykewicz, A.J., H.S. Isaacs, and A.J. Davenport. 1995. *Journal of the Electrochemical Society* **142** [10], 3342.
- American Society for Testing and Materials. 1995a. A516-90. Standard specification for pressure vessel plates, carbon steels for moderate- and lower-temperature service. *Annual Book of ASTM Standards*. Philadelphia, PA: American Society for Testing and Materials: Vol. 01.04: 248-250.
- American Society for Testing and Materials. 1995b. A387-92. Standard specification for pressure vessel plates, alloy steel, chromium-molybdenum. *Annual Book of ASTM Standards*. Philadelphia, PA: American Society for Testing and Materials: Vol. 01.04: 210-212.
- Bittner, H.F., J.T. Bell, J.D. Redman, W.H. Christie, and R.B. Eby. 1980. *Metallurgical Transactions* **11A**, 783.
- Boggs, W.E., and R.H. Kachik. 1969. *Journal of the Electrochemical Society* **116** [4], 424.
- Boggs, W.E., R.H. Kachik, and G.E. Pellissier. 1965. *Journal of the Electrochemical Society* **112**, 539.
- Boggs, W.E., R.H. Kachik, and G.E. Pellissier. 1967. *Journal of the Electrochemical Society* **114**, 32.
- Caplan, D., and M. Cohen. 1963. *Corrosion Science* **3**, 139.
- Caplan, D., and M. Cohen. 1966. *Corrosion Science* **6**, 321.
- Caplan, D., M.J. Graham, and M. Cohen. 1970a. *Corrosion Science* **10**, 1.
- Caplan, D., G.I. Sproule, and R.J. Hussey. 1970b. *Corrosion Science* **10**, 9.
- Caplan, D., G.I. Sproule, R.J. Hussey, and M.J. Graham. 1978. *Oxidation of Metals* **12** [1], 67.
- Christl, W., A. Rahmel, and M. Schutze. 1989. *Oxidation of Metals* **31** [1/2], 1.
- Cotell, C.M., G.J. Yurek, R.J. Hussey, D.F. Mitchell, and M.J. Graham. 1990. *Oxidation of Metals* **34**, 173.
- Craig, B.D., ed. 1989. *Handbook of Corrosion Data*, ASM International, Materials Park, Ohio.
- Davenport, A.J., H.S. Isaacs, and M.W. Kendig. 1991. *Corrosion Science* **32**, 653.
- Davies, D., U.R. Evans, and J. Agar. 1954. *Proceedings of the Royal Society of London*, **A225**, 443.
- Davis, J.R., ed. 1996. *Carbon and Alloy Steels*, ASM Specialty Handbook, ASM International, Materials Park, Ohio.

- Dieckmann, R., and H. Schmalzried. 1977. *Berichte der Bunsengesellschaft für Physikalische Chemie* **81**, 344.
- Douglass, D.L., F. Gesmundo, and C. DeAsmundis. 1986. *Oxidation of Metals* **25** [3/4], 235.
- Fromhold, A.T., Jr., and N. Sato. 1981. *Oxidation of Metals* **16** [3/4], 203.
- Fromhold, A.T., Jr. 1982. *Journal of Physics and Chemistry of Solids* **43**, 405.
- Funkenbusch, A.W., J.G. Smeggil, and N.S. Bornstein. 1985. *Metallurgical Transactions* **16A**, 1164.
- Giggins, C.S., and F.S. Pettit. 1969. *Transactions of the Metallurgical Society of AIME* **245**, 2509.
- Gonzales, J.J., D. Oquab, and B. Pieraggi. 1996. Personal communication.
- Grabke, H.J., K. Ohla, J. Peters, and I. Wolf. 1983. *Werkstoffe und Korrosion* **34**, 495.
- Grabke, H.J., D. Wiemer, and H. Viehhaus. 1991. *Applications of Surface Science* **47**, 243.
- Graham, M.J., and M. Cohen. 1969. *Journal of the Electrochemical Society* **116**, 1430.
- Grauer, R., and W. Feitknecht. 1966. *Corrosion Science* **6**, 301.
- Himmel, L., R.F. Mehl, and C.E. Birchenall. 1953. *Journal of Metals* **5**, 827.
- Hirth, J.P., B. Pieraggi, and R.A. Rapp. 1995. *Acta Metallurgica et Materialia* **43** [3], 1065.
- Holmes, D.R., R.B. Hill, and L.M. Wyatt, ed. 1974. *Corrosion of Steels in CO₂*, British Nuclear Energy Society, London, UK.
- Hsu, H.S. 1986. *Oxidation of Metals* **26**, 315.
- Hurdus, M.H., L. Tomlinson, and J.M. Titchmarsh. 1990. *Oxidation of Metals* **34** [5/6], 429.
- Hussey, R.J., and M. Cohen. 1971a. *Corrosion Science* **11**, 713.
- Hussey, R.J., and M. Cohen. 1971b. *Corrosion Science* **11**, 699.
- Hussey, R.J., G.I. Sproule, D. Caplan, and M.J. Graham. 1977. *Oxidation of Metals* **11** [2], 65.
- Hussey, R.J., P. Papaiavocou, J. Shen, D.F. Mitchell, and M.J. Graham. 1989. *Materials Science and Engineering* **A120**, 147.
- Jha, B.B., B. Raj, and A.S. Khanna. 1986. *Oxidation of Metals* **26** [3/4] 263.
- Khanna A.S., and K.P. Singh. 1982. *Transactions of the Indian Institute of Metals* **35** [5], 494 .
- Khanna A.S., and J.B. Gnanamoorthy. 1982. *Oxidation of Metals* **18** [5/6].

- Khanna, A.S., B.B. Jha, and B. Raj. 1985. *Oxidation of Metals* **23** [3/4], 159.
- Khanna, A.S., R.K.S. Raman, and J.B. Gnanamoorthy. 1987. *10th International Congress of Metallic Corrosion*. ICMC-10, Vol. IV. Central Electrochemical Research Institute, Karaikudi, India, TransTech Publications, Switzerland, p. 3453.
- Klotsman, S.M., A.N. Timofeyev, and I.S. Trakhtenberg. 1960. *Physics of Metals and Metallography* **10**, 93.
- Kokowa, M., and S. Nagata. 1981. *Corrosion Science* **21**, 819.
- Kofstad, P. 1988. *High-Temperature Corrosion*, Elsevier Science Publishers, New York, New York.
- Leistikow, S., I. Wolf, and H.J. Grabke. 1987. *Werkstoffe und Korrosion* **38**, 556.
- Mackenbrock, M., and H.J. Grabke. 1992. *Materials Science and Technology* **8**, 541.
- Mackenzie, J.D., and C.E. Birchenall. 1957. *Corrosion* **13**, 783.
- Mansfeld, F., S. Lin, S. Kim, and H. Shih. 1990. *Journal of the Electrochemical Society* **137**, 78.
- McLean, D. 1957. *Grain Boundaries in Metals*, Oxford University Press, New York.
- McMahon, C.J., Jr. 1968. "Temper Brittleness—An interpretative review." *Temper Embrittlement in Steel*, ASTM, Philadelphia PA, 127.
- Mintz, B., H. Ke, and G.D.W. Smith. 1992. *Materials Science and Technology* **8**, 537.
- Misra, R.D.K., and P.R. Rao. 1992. *Acta Metallurgica et Materialia*, **40** [6], 1223.
- Moon, D.P. 1989. *Materials Science and Technology* **5**, 754.
- Muan A., and E.F. Osborn. 1965. *Phase Equilibria Among Oxides in Steelmaking*, Addison-Wesley Publishing Company, Inc., Reading, MA.
- Murza, J.C., and C.J. McMahon, Jr. 1980. *Journal of Engineering Materials and Technology* **102**, 369.
- Nuttall, K., and V.F. Urbanic. 1981. "An Assessment of Materials for Nuclear Fuel Immobilization Containers," AECL-6440, Atomic Energy of Canada, Ltd.
- Ohtani, H., and C.J. McMahon, Jr. 1975. *Acta Metallurgica* **23**, 377.
- Païdassi, J. 1958. *Acta Metallurgica* **6**, 184.
- Patibandla, N., T.A. Ramanarayanan, and F. Cosandey. 1991. *Journal of the Electrochemical Society* **138** [7], 2176.
- Perrow, J.M., W.W. Smeltzer, and J.D. Embury. 1968. *Acta Metallurgica* **16**, 1209

- Pieraggi, B. 1987. *Oxidation of Metals* 27 [3/4], 177.
- Pieraggi, B., and R.A. Rapp. 1993. *Journal of the Electrochemical Society* 140 [10], 2844.
- Pieraggi, B., and R.A. Rapp. 1988. *Acta Metallurgica* 36 [5], 1281.
- Pieraggi, B., R.A. Rapp, and J.P. Hirth. 1995. *Oxidation of Metals* 44 [1/2], 63.
- Pilling J., and N. Ridley. 1982. *Metallurgical Transactions* 13A, 557.
- Pint, B.A. 1996. *Oxidation of Metals* 45, 1.
- Pourbaix, M., H. Zhang, and X. Yang. 1996. *Atlas of Chemical and Electrochemical Equilibria in the Presence of a Gaseous Phase*, ed. Cebelcor, Brussels.
- Prescott, G.R. 1980. Materials problems in the hydrogen-carbon processing industries. *Alloys for the Eighties*, R.Q. Barr, ed., Climax Molybdenum Company, 303.
- Price, W.R. 1967. *Corrosion Science* 7, 473.
- Przybylski, K., A.J. Garatt-Reed, and G.J. Yurek. 1988. *Journal of the Electrochemical Society* 135, 509.
- Rahmel, A. 1961. *Mitteilungen VGB* 74, 319.
- Raman, R.K.S., A.S. Khanna, and J.B. Gnanamoorthy. 1988. *Oxidation of Metals* 30 [5/6] 345.
- Raman, R.K.S., A.S. Khanna, R.K. Tiwari, and J.B. Gnanamoorthy. 1992. *Oxidation of Metals* 37 [1/2], 1.
- Rapp, R.A. 1980. *High Temperature Corrosion* (reference manual for Audio Course), The American Chemical Society, Washington, DC.
- Rellick, J.R., and C.J. McMahon, Jr. 1974. *Metallurgical Transactions* 5, 2439.
- Runk, R.B., and H.J. Kim. 1970. *Oxidation of Metals* 2 [3], 285
- Shewmon, P.G. 1976. *Metallurgical Transactions* 7A, 279.
- Shida, Y., N. Ohtsuka, J. Murayama, N. Fujino, and H. Fujikawa. 1983. *Proceedings of the International Symposium on High Temperature Corrosion. JIMIS-3*, Japan Institute of Metals, 63.
- Simmons, G.W., E. Kellerman, and H. Leidheiser. 1973. *Corrosion* 29, 227.
- Simms, N.J., and J.A. Little. 1987. *Oxidation of Metals* 27 [5/6] 283.
- Smeggil, J.G., A.W. Funkenbusch, and N.S. Bornstein. 1986. *Metallurgical Transactions* 17A, 923.

- Smialek, J.L. 1991. *Metallurgical Transactions* **22A**, 739.
- Strawbridge, A., and R.A. Rapp. 1994. *Journal of the Electrochemical Society* **141** [7], 1905.
- Strawbridge, A., R.A. Rapp, G.I. Sproule, R.J. Hussey, and M.J. Graham. 1995. *Journal of the Electrochemical Society* **141** [7], 2301.
- Stringer, J. 1989. *Materials Science and Engineering* **A120**, 129.
- Sundarajan, G., and P.G. Shewmon. 1981. *Metallurgical Transactions* **12A**, 1761.
- Takayama, S., T. Ogura, S.-C. Fu, and C.J. McMahon, Jr. 1980. *Metallurgical Transactions* **11A**, 1513.
- Tomlinson, L., M.H. Hurdus, P.J.B. Silver, and W. Lilley. 1978. *Proceedings of the International Conference on Ferritic Steels of Fast Reactor Steam Generators*, British Nuclear Energy Society, London, UK, 353.
- TRW Environmental Safety Systems, Inc. 1995. *Total System Performance Assessment—1995: An Evaluation of the Potential Yucca Mountain Repository*. B00000000-01717-2200-00136, Rev. 01. Las Vegas, NV: TRW Environmental Safety Systems, Inc.
- TRW Environmental Safety Systems, Inc. 1996. *Mined Geologic Disposal System Advanced Conceptual Design Report. Engineered Barrier Segment/Waste Package*. B00000000-01717-5705-00027, Rev. 00. Las Vegas, NV: TRW Environmental Safety Systems, Inc.
- Ucisik, A.H., C.J. McMahon, Jr., and H.C. Feng. 1978. *Metallurgical Transactions* **9A**, 321.
- Uhlig, H.H. 1956. *Acta Metallurgica* **4**, 541.
- Van Konynenburg, W.G. Halsey, R.D. McCright, W.L. Clark, and G. Gdowski. 1993. *Selection of Candidate Materials for the Conceptual Waste Package Design for a Potential High Level Nuclear Waste Repository at Yucca Mountain*, UCRL-ID-112058, Lawrence Livermore National Laboratory, Livermore, CA.
- Vernon, W.H., E.A. Calnan, C.J. Clews, and T.J. Nurse. 1953. *Proceedings of the Royal Society of London*, **A216**, 375.
- Viani, F., and F. Gesmundo. 1980. *Corrosion Science* **20**, 541.
- Wagner, C. 1951. *Atom Movements*, American Society for Metals, Metals Park, OH, 153.
- Wagner, C. 1969. *Acta Metallurgica* **17**, 99.
- Wang, G., B. Gleeson, and D.L. Douglass. 1989. *Oxidation of Metals* **31** [5/6], 415.
- Webb, W.W., J.T. Norton, and C. Wagner. 1956. *Journal of the Electrochemical Society* **103**, 112.

- Whittle, D.P., and J. Stringer. 1980. *Philosophical Transactions of the Royal Society* **A295**, 309.
- Wolf, I., and H.J. Grabke. 1985. *Solid State Communications* **54**, 5.
- Yearian, H.J., E.C. Randell, and T.A. Longo. 1956. *Corrosion* **12**, 515.
- Yu, J., and C.J. McMahon, Jr. 1980a. *Metallurgical Transactions* **11A**, 277.
- Yu, J., and C.J. McMahon, Jr. 1980b. *Metallurgical Transactions* **11A**, 291.
- Yurek, G.J., J.P. Hirth, and R.A. Rapp. 1974. *Oxidation of Metals* **8**, 263.